Electrochemical Protein Detection Exploring Redox Cation-DNA Interaction for Signal Enhancement

by

Ping Li

B.Sc., Nankai University, 2012

Thesis Submitted in Partial Fulfillment of the
Requirements for the Degree of
Master of Science

in the
Department of Chemistry
Faculty of Science

SIMON FRASER UNIVERSITY

Fall 2015

Approval

Name: **Ping Li**

Degree: **Master of Science**

Title: ***Electrochemical Protein Detection Exploring Redox Cation-DNA Interaction for Signal Enhancement***

Examining Committee: **Chair:** Krzysztof Starosta
Associate Professor

Hua-Zhong Yu
Senior Supervisor
Professor

Dipankar Sen
Supervisor
Professor

Michael Eikerling
Supervisor
Professor

Loren Kaake
Internal Examiner
Assistant Professor

Date Defended/Approved: December 8, 2015

Abstract

A simple DNA-redox cation interaction enhancement strategy has been developed for improving the sensitivity of electrochemical immunosensors for protein detection. Instead of labeling with fluorophores or redox-active groups, the detection antibodies were tethered with DNA single strands. Based on the electrostatic interaction between redox cations ($[Ru(NH_3)_6]^{3+}$) and negatively charged DNA backbone, enhanced electrochemical signals were obtained. Human chorionic gonadotropin (hCG) detection has been performed as a trial analysis. A linear response up to 25 mIU/mL and a detection limit of 1.25 mIU/mL have been achieved, both comparable with standard enzyme-linked immunosorbent assay (ELISA) tests. The method also shows remarkable selectivity towards hCG over other hormones such as thyroid stimulating hormone (TSH) and follicle stimulating hormone (FSH). By and large, our approach bears the merits of cost effectiveness and simplicity of instrumentation in comparison with conventional optical detection methods.

Keywords: electrochemical immunoassay; redox labeling; signal enhancement; DNA-cation interaction; hCG

This thesis is dedicated to my family and friends for their endless love, support and encouragement.

Acknowledgements

Firstly I would like to thank my senior supervisor Dr. Hua-Zhong (Hogan) Yu for his patient guidance, advice and support throughout the past years. It would be impossible for me to finish this work without his help. I benefit a lot from the discussions with him. I am grateful to Dr. Yu for giving me this research opportunity in 4D Labs at SFU, which is such a fantastic place to get access to all these advanced techniques and facilities. Also, it is a great honor for me to work in Dr. Yu's lab and meet the current and past members of the Yu group. They are incredibly brilliant and friendly. I truly appreciate the invaluable friendship and constant encouragement from them.

I also would like to express my sincere gratitude to Dr. Bixia Ge for her training and helpful suggestions. She taught me many experimental skills and helped me to solve lots of problems I met during my research.

In addition, special thanks to Dr. Dipankar Sen and Dr. Michael Eikerling for being my committee members. Their questions and suggestions greatly helped me to better understand my project and to improve my knowledge of biochemistry and electrochemistry. I also would like to thank Dr. Eberhard Kiehlmann for proofreading the manuscript. I sincerely appreciate all the help.

Last but not least, I would like to thank my parents for their unconditional love and support. I always know they believe in me and want the best for me. Thank you.

Table of Contents

List of Tables

List of Figures

List of Acronyms

A	adenosine nucleoside
AuNPs	gold nanoparticles
BSA	bovine serum albumin
C	cytidine nucleoside
CC	chronocoulometry
cDNA	complementary DNA
CEA	carcinoembryonic antigen
CV	cyclic voltammetry
DNA	deoxyribose nucleic acid
dsDNA	double-stranded DNA
EDC	1-ethyl-3-(3-dimethylaminopropyl) carbodiimide hydrochloride
ELISA	enzyme-linked immunosorbent assay
Fc	ferrocene
FSH	follicle stimulating hormone
G	guanosine nucleoside
hCG	human chorionic gonadotropin
HCP	hybridization chain reaction
HIgG	human immunoglobulin G
HRP	horseradish peroxidase
IL-6	interleukin-6
LFA	lateral-flow assay
LH	luteinizing hormone
Mab	monoclonal antibody
MB	methylene blue
MCH	1-mercapto-6-hexanol
MCHA	6-mercaptohexanoic acid
MES	N-morpholinoethane sulfonic acid
MPs	superparamagnetic particles
MUC1	mucin 1
MWCNTs	multiwalled carbon nanotubes
NHS	N-hydroxysuccinimide

PBS	phosphate buffered saline
POC	point of care
PSA	prostate specific antigen
rGO	reduced graphene oxide
S.H.E.	standard hydrogen electrode
SAM	self-assembled monolayer
ssDNA	single-stranded DNA
T	thymidine nucleoside
TMB	3,3’,5,5’-tetramethylbenzidine
Tris	tris(hydroxylmethyl)aminomethane
TSH	thyroid stimulating hormone
UV	ultraviolet

Chapter 1.

Introduction

The immunoassay has been one of the most active research topics for several decades. Because of the biospecific recognition between antibody and antigen, this method has wide applications in bioanalysis and clinical chemistry. Among all the immunoassay techniques, electrochemical immunosensors exhibit the merits of cost effectiveness, good portability as well as high sensitivity. In this chapter, a general introduction to the redox labeling method and to the immunoassay is provided. It also summarizes the efforts that have been made to develop new labeling methods as well as electrochemical immunosensors for the increasing needs of high sensitivity (low detection limit) and multiplex tests in a signal trial.

Since human chorionic gonadotropin (hCG) detection has often been studied as a model system, a brief introduction of hCG will also be presented. In addition, this chapter provides background information and explains fundamental electrochemical concepts, which form the basis of the work described in this thesis.

1.1. DNA-cation interaction and electrochemical characterization

1.1.1. Cyclic voltammetry: from solution to surface

The word “redox” is short for “reduction and oxidation”, which identifies two processes involved in a redox reaction.[1] Back to two centuries ago, the term oxidation was coined for reactions with oxygen. Later it was recognized that many compounds of oxygen can also bring about oxidation reactions just like oxygen itself. Since the discovery of the electron in 1897, the definition of oxidation became broader, and came

to refer to a loss of electrons. In the meantime, reduction was defined to be “gain of electrons.”[2] An oxidation reaction alone and a reduction reaction alone are called half-reactions, which means that a whole redox reaction is composed of two half-reactions; neither oxidation nor reduction can take place without the other one.[3]

Redox reactions are characterized by electron transfer. The oxidizing agent is the molecule or ion that accepts electrons and oxidizes other substances while it is itself reduced. The reducing agent has the ability of donating electrons and thus is itself oxidized.[4] (Figure 1-1)

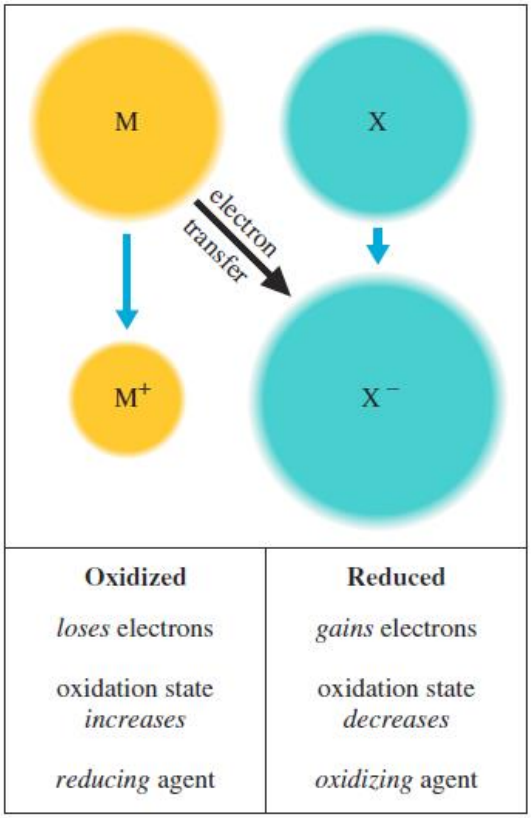

Figure 1.1. Schematic view of a redox process, in which M is oxidized and X is reduced.

Note. Reprinted with permission from Zumdahl, S.; DeCoste, D. J. Chemical Principles; 7th ed.; Brooks/Cole, Cengage Learning: Belmont, CA, 2013. Copyright 2013 Cengage Learning.

As shown in Figure 1-1, a redox reaction involves an electron transfer from the reducing agent to the oxidizing agent, which can be analyzed as two half-reactions as noted above.[3] Each half-reaction has a standard reduction potential, E° at 25° C (298 K).

To determine the standard reduction potential value for common half-reactions, the potential of a standard hydrogen electrode is used as reference. The reaction of the standard hydrogen electrode is

$$2H^+ + 2e^- \rightarrow H_2 \quad (1\text{-}1)$$

where $[H^+]$ = 1 M and P_{H2} = 1 atm. The potential of this reaction has been defined to be 0. By using the standard hydrogen electrode (S.H.E.) as reference, common standard reduction potentials have been measured and summarized in the literature. A more positive standard electrode potential indicates a stronger oxidizing ability.

By using the two half-reactions, a balanced redox reaction potential can be determined by the following equation:

$$E^\circ_{cell} = E^\circ(\text{cathode}) - E^\circ(\text{anode}) \quad (1\text{-}2)$$

where the cathode is the site where reduction occurs and the anode refers to the oxidation site.[5]

The oxidizing agent and the reducing agent are usually placed separately and linked together by an external circuit to allow the electrons to flow from one side to the other side.[6] Such a device is named a galvanic cell, in honor of the Italian scientist Luigi Galvani. The batteries and fuel cells we are using today are both galvanic cells that generate electricity by spontaneous chemical redox reactions.[7]

The standard reduction potential defines the redox ability under standard conditions. In order to monitor the electrode potential of a half-reaction at any point in time under non-standard conditions, the Nernst equation is required. It expresses the relationship between a half-cell reduction potential E and its standard reduction potential E° as well as the influence of temperature T, species activity α and reaction quotient Q. For the half-reaction

$$ox + ne^- \rightarrow red \quad (1\text{-}3)$$

the Nernst equation can be written as

$$E = E^{\circ} + \frac{RT}{nF} \ln \frac{\alpha_{ox}}{\alpha_{red}} \quad (1\text{-}4)$$

where E° is the standard reduction potential; R is the gas constant (8.314 J/ (K·mol)); T is the temperature (K); n is the number of electrons in the half-reaction; F is the Faraday constant (9.649 $\times 10^4$ C/ mol); and α is the chemical activity of the species of interest. When the temperature is 25 °C, the Nernst equation is simplified to

$$E = E^{\circ} + \frac{0.05916}{n} \log \frac{\alpha_{ox}}{\alpha_{red}} \quad (1\text{-}5)$$

The relationship between equilibrium constant and cell potential can also be calculated from the Nernst equation. If electrons flow from the left electrode to the right electrode, the two half-reactions are:

$$\text{right electrode (cathode): } aA + ne^- \leftrightarrow cC \quad (1\text{-}6)$$

$$\text{left electrode (anode): } dD + ne^- \leftrightarrow bB \quad (1\text{-}7)$$

The Nernst equation can be written as:

$$E = E_{cat} - E_{and} = E^{\circ}_{cat} - \frac{0.05916}{n} \log \frac{\alpha_C^c}{\alpha_{aA}^a} - \left(E^{\circ}_{and} - \frac{0.05916}{n} \log \frac{\alpha_B^b}{\alpha_D^d}\right) \quad (1\text{-}8)$$

$$E = \left(E^{\circ}_{cat} - E^{\circ}_{and}\right) - \frac{0.05916}{n} \log \left(\frac{\alpha_C^c}{\alpha_{aA}^a} \cdot \frac{\alpha_B^b}{\alpha_D^d}\right) = E^{\circ} - \frac{0.05916}{n} \log Q \quad (1\text{-}9)$$

where Q is the reaction quotient. When equilibrium has been reached, the reduction potential E equals 0 and Q is equal to the equilibrium constant K. In this way, equation (1-10) can be further transformed into

$$E^{\circ} = \frac{0.05916}{n} \log K \quad (1\text{-}10)$$

Therefore, the standard electrode potential and the equilibrium constant of a redox reaction are related.

Cyclic voltammetry is one of the most popular methods to exam electroactive species because of the simplicity of measurement and easy interpretation of the data. Wide applications in electrochemistry, inorganic chemistry, organic chemistry, and biochemistry have proved the versatility of this technique.[8] Cyclic voltammetry measures the response current after applying a cycling potential on the electrodes that are immersed in the solution of interest. To be more specific, starting from an initial voltage on the working electrode, the potential will be scanned linearly with a defined scan rate (V/s) towards a pre-set switch point, where the scan direction is reversed; this way the potential gets cycled. With the help of a reference electrode, such as a saturated calomel electrode or a silver | silver chloride electrode, the potential of the working electrode can be regulated. The scan rate can be set up according to experimental conditions.

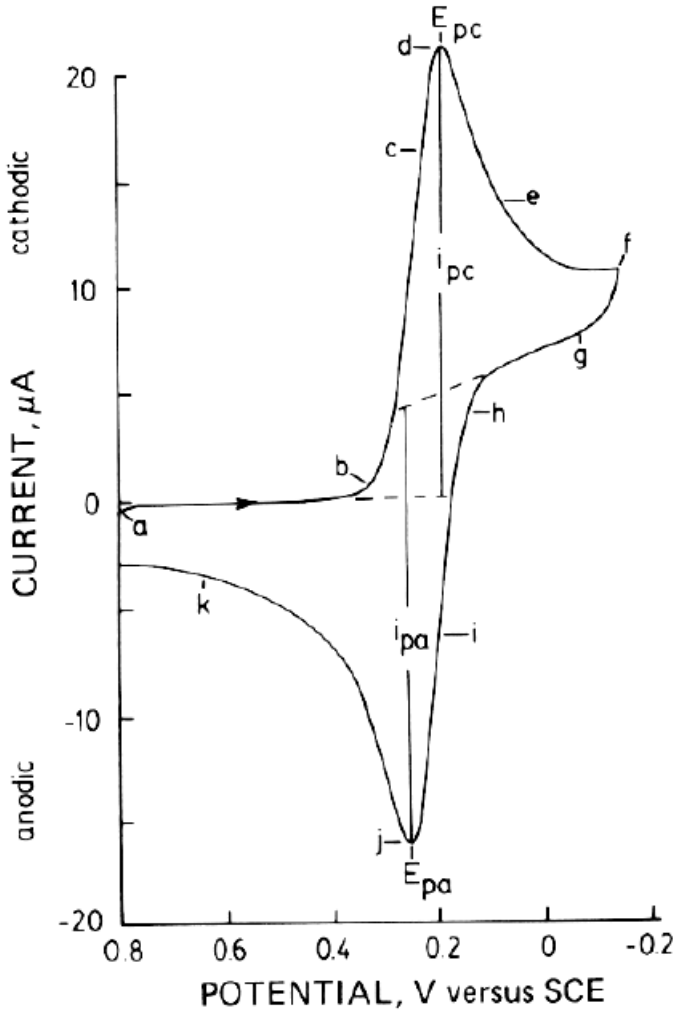

Figure 1.2. Cyclic voltammogram of the $Fe(CN)_6^{3-}$/ $Fe(CN)_6^{4-}$ redox reaction. The initial potential is labeled as "a" and the turning point is labeled as "f". The cathodic peak and the anodic peak are represented by E_{pc} and E_{pa}, respectively. The scan direction is indicated by the black arrow.

Note. Reprinted with permission from Kissinger, P. T.; Heineman, W. R. Cyclic Voltammetry. *J. Chem. Educ.* 1983, *60*, 702–706. Copyright 1983 American Chemical Society.

In Figure 1.3 the initial potential is chosen as 0.8 V to avoid the electrolysis of $Fe(CN)_6^{3-}$ when the electrode is switched on. The potential goes towards the negative direction. When the potential is negative enough to reduce $Fe(CN)_6^{3-}$, the current starts to increase rapidly and reached maximum at the potential of E_{pc}. As diffusion is too slow to replenish analyte from the bulk solution, the $Fe(CN)_6^{3-}$ near the electrode becomes depleted, resulting in a decreased cathodic current at more negative potentials. When

the switch point is reached, the scan potential is reversed. Since the potential on the working electrode is still negative enough to reduce $Fe(CN)_6^{3-}$, the current continues even when the potential scans towards the positive direction. When the potential on the working electrode is positive enough to oxidize the reduced product $Fe(CN)_6^{4-}$, the current starts to increase rapidly again until the surface concentration of reduced analyte $Fe(CN)_6^{4-}$ is depleted. The anodic current decays back to a small value as the solution surrounding the electrode is depleted of $Fe(CN)_6^{4-}$. In this way, the electroactive species $Fe(CN)_6^{3-}$ is first reduced to $Fe(CN)_6^{4-}$ while generating the cathodic current, then oxidized back to $Fe(CN)_6^{3-}$ as indicated by the anodic current.

The Nernst equation for the electroactive pair $Fe(CN)_6^{3-}$/ $Fe(CN)_6^{4-}$ illustrates the relationship between the potential that is applied to the working electrode and the concentration change of $Fe(CN)_6^{3-}$ and $Fe(CN)_6^{4-}$ at the electrode surface. As the potential changes towards the negative direction, the concentration ratio $Fe(CN)_6^{3-}$ / $Fe(CN)_6^{4-}$ has to be changed to satisfy the Nernst equation; in other words, the concentration of $Fe(CN)_6^{3-}$ at the electrode surface decreases. The reduction of $Fe(CN)_6^{3-}$ to $Fe(CN)_6^{4-}$ helps to reduce the concentration of $Fe(CN)_6^{3-}$ while increasing the concentration of $Fe(CN)_6^{4-}$ at the electrode surface. This ratio keeps changing according to the different potentials that are applied to the electrode to satisfy the Nernst equation at any particular point during the whole scanning process. When the applied potential E equals E°', the concentration ratio $Fe(CN)_6^{3-}$ / $Fe(CN)_6^{4-}$ equals 1 according to the equation. The rapidly increasing cathodic current in the region b-d reflects the logarithmic relationship between E and $[Fe(CN)_6^{3-}]$ / $[Fe(CN)_6^{4-}]$

When the potential reaches its pre-set switch point, the scan direction turns backwards. During the depletion of $Fe(CN)_6^{3-}$ at the electrode, the amount of $Fe(CN)_6^{4-}$ is increasing. Although the scan direction becomes positive, the reduction continues as the potential is still sufficiently negative. When the applied potential is positive enough to oxidize $Fe(CN)_6^{4-}$, the anodic current starts to increase rapidly. The formation of a peak indicates the depletion of $Fe(CN)_6^{4-}$ at the electrode surface. At this point the anodic current starts to decrease.

The peak current serves as another important parameter in a cyclic voltammogram. By analyzing the symmetry of peak currents, a redox reaction is reversible or irreversible can be found out.

As shown in Figure 1.2, the cathodic peak and the anodic peak are symmetric accompany with the same intensity of peak currents, which illustrates a reversible reaction. For a reversible reaction, an equilibrium between reactant and product at the electrode surface can be established because of the fast reaction rate.[5] Also, for a reversible reaction, the relationship between cathodic peak potential and anodic peak potential obeys the equation (1-11) at 25 °C:[9]

$$\mathrm{E_{pa}} - \mathrm{E_{pc}} = \frac{2.22\mathrm{RT}}{\mathrm{nF}} = \frac{57.0}{\mathrm{n}}\ (mV) \tag{1-11}$$

where E_{pa} and E_{pc} are the potentials where anodic peak current and cathodic peak current are measured and n is the number of electrons in the half-reaction. Therefore, for a one-electron process such as the reduction of $Fe(CN)_6^{3-}$ to $Fe(CN)_6^{4-}$, the peak separation should be around 0.057 V. For an irreversible reaction, the separation between cathodic and anodic peak is larger due to the slow electron transfer rate.

In a reversible reaction, the peak current of the forward sweep of the first cycle can be presented by the Randles-Sevcik equation,[9]

$$\mathrm{I_{pc}} = (2.69 \times 10^8)\mathrm{n}^{3/2}\mathrm{ACD}^{1/2}\mathrm{v}^{1/2} \tag{1-12}$$

where n is the number of electrons in the half reaction, A is the surface area of the electrode (m^2), C is the concentration (mol/L), D is the diffusion coefficient of the electroactive species (m^2/s), and v is the scan rate (V/s). I_{pc} is proportional to the $v^{1/2}$ when other conditions remain the same. If the electroactive species is adsorbed on the electrode, the peak current is proportional to the scan rate v instead of $v^{1/2}$. For the irreversible redox reaction, the electron exchange rate of the redox species at the electrode is very slow. Therefore, the aforementioned equations (1-11), (1-12) cannot be applied.

The aforementioned electroactive pair $Fe(CN)_6^{3-}$/ $Fe(CN)_6^{4-}$ is dissolved in the solution. As for the electroactive species that are adsorbed onto the electrode, the interpretation is different. In this case, the scan rate is so fast that there is no time for the redox species to diffuse appreciably to the electrode surface. At very low solution concentrations, adsorption between redox species and electrode can be so strong that the dissolved redox species barely affects the signaling current.[10]

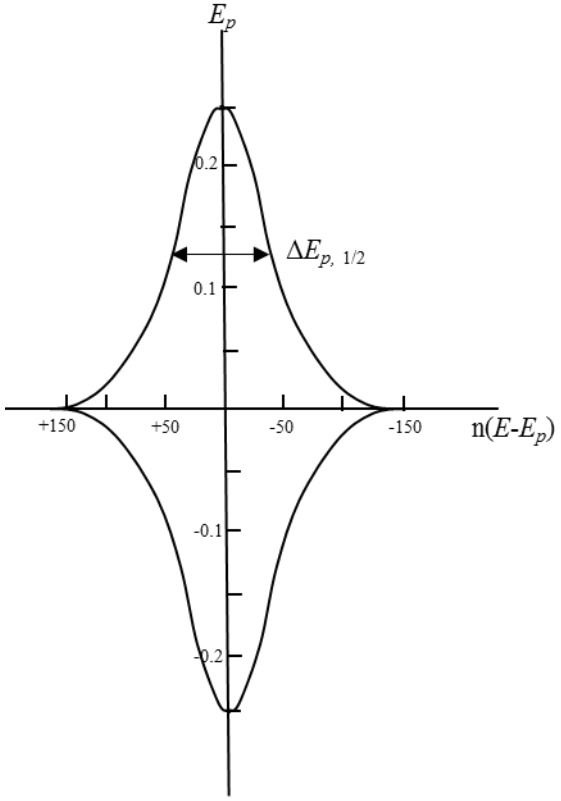

Figure 1.3. Cyclic voltammogram for redox reaction of adsorbed electroactive species. (normalized current and potential axis at 25 °C).

In this situation, the peak current is proportional to the scan rate v instead of $v^{1/2}$. By integrating the peak current, the charge that is needed for complete reduction of the adsorbed layer can be calculated. The peak current follows the equation:

$$i_p = \frac{n^2F^2}{4RT} vA\Gamma_o^* \qquad (1\text{-}13)$$

where Γ_O^* refers to the total surface density of the adsorbed species. For an ideal Nernstian reaction that follows the Langmuir isotherm, $E_{pa} = E_{pc}$. The total width at high cathodic peak height can be defined as:

$$\Delta E_{p,1/2} = 3.53 \frac{RT}{nF} = \frac{90.6}{n}\ mV\ (25℃) \quad (1\text{-}14)$$

All in all, by using cyclic voltammetry, redox behavior and kinetics properties of a certain target can be studied. It offers a fast and easy way to understand the electrochemical readout.

1.1.2. DNA-ligand interaction and redox labeling

Bearing the merits of high throughput, simple fabrication, and high accuracy, DNA-based biosensors and microarrays have drawn attention for many decades. The wide applications in various fields such as DNA diagnostics, environmental safety monitoring, and ion detection provide a huge motivation for further development in this area.[11] Labeling DNA probes with different kinds of tags is essential in order to meet different demands. Generally there are three methods of labeling DNA probes: radiolabeling, fluorescence labeling, and redox labeling.[12] Considering the drawback of expensive reagents and the advanced equipment needed for conventional fluorescence and radiolabel-based DNA sensors, redox-labeled DNA sensors show advantages in cost effectiveness, good portability, and excellent sensitivity.[13]

For redox labeled DNA sensors, the most frequently used electrode is gold, on which the thiolated DNA or alkanethiols can be immobilized through strong Au-S bond.[14] In order to precisely control the surface density, a mixed monolayer can be created by mixing DNA strands and short alkanethiols such as mercaptohexanol (MCH).

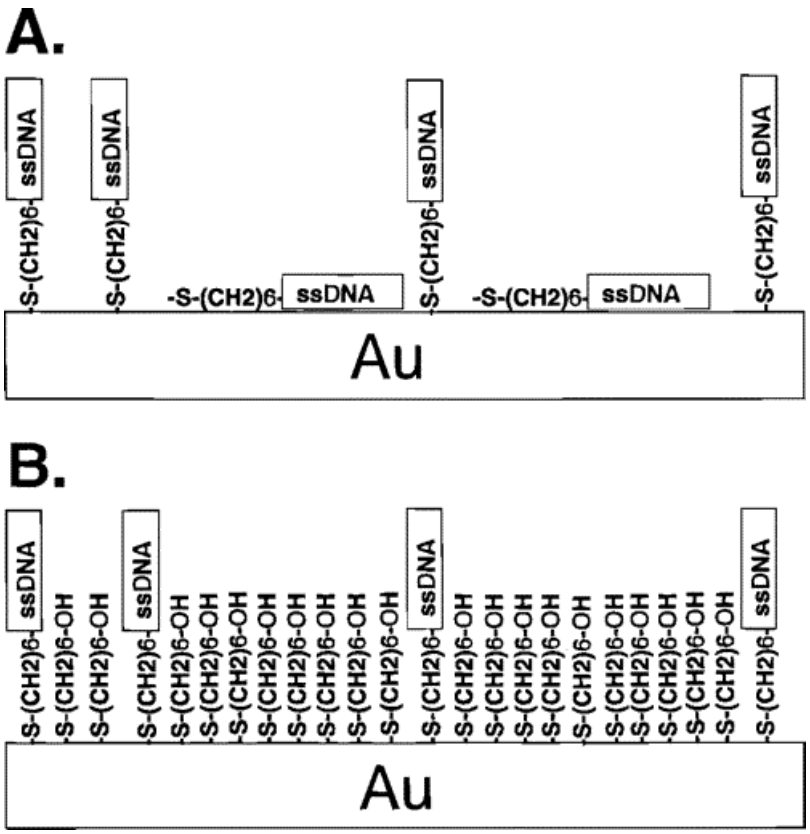

Figure 1.4. DNA monolayers on gold (A) without mercapto alchohol and (B) with alkanethiol spacers. 1-Mercapto-6-hexanol (MCH) is used as example.

Note. Reprinted from Herne, T. M.; Tarlov, M. J. Characterization of DNA Probes Immobilized on Gold Surfaces. *J Am Chem Soc* 1997, *119*, 8916–8920. Copyright 1997 American Chemical Society.

The gold substrate is typically first incubated in thiolated DNA and later exposed to a high concentration of MCH solution. In this way, the nonspecific adsorbed DNA strands will be largely removed from the surface, leaving a more ordered surface bound DNA/MCH monolayer. The DNA chips modified by this two-step method were proved to be stable and also showed high hybridization efficiency with complementary DNA.[15] Compared with the pure DNA-modified gold electrodes, the mixed monolayer yields a significantly better electrochemical response.[16] The use of longer mercapto- alchohols as spacers helps to form more stable electrodes for long-term dry storage while the shorter ones offer better electron transfer properties.[17]

In general, there are three types of interactions between redox molecules and DNA strands that can be adapted for DNA redox labeling: covalent bonding, intercalation, and electrostatic interaction. Depending on different demands, the redox reporter can be attached to the DNA strands through a covalent linker or get to DNA strands through solution diffusion. The signals given by the redox reaction of the reporter molecules are then recorded and compared to study the properties of the modified surface.

Covalently tethered: Some redox reporters, such as methylene blue (MB) and ferrocene (Fc) can be covalently attached to DNA strands through a flexible alkyl linker. This strategy ensures that the placement of the DNA probes will not be hindered by the redox molecules and also helps to build high quality DNA films.[18] It is easier to control the position of the redox reporters because the mobility of the redox reporter has been restricted. Also, the influence from the diffusion process can be considered as negligible due to the fact that the reporter has been linked to the surface-bound DNA strands; only the surface-controlled process is considered, which helps to simplify the data analysis process. Additionally, the number of redox reporters per DNA strand is known and fixed, so that the amount of surface-bound DNA can be calculated from the electrochemical signals of the redox reporters.

There is a well-established protocol for preparing MB-labeled DNA strands. The amino-modified DNA oligonucleotides are incubated with freshly made N-hydroxysuccinimide (NHS) ester of N-(carboxypropyl)methylene blue. The chemical structure is shown below.[18]

Figure 1.5. The chemical structure of MB-tethered DNA.

Note. Reprinted with permission from Pheeney, C. G.; Barton, J. K. DNA Electrochemistry with Tethered Methylene Blue. *Langmuir* 2012, *28*, 7063–7070. Copyright 2012 American Chemical Society.

The DNA probes with covalently tethered redox reporter have wide applications in various fields, such as fundamental electrochemical studies of DNA-modified surfaces,[19] environmental monitoring,[20] and detection of biomarkers.[21] As shown in Figure 1.4, the proposed DNA sensor was used for detecting the tumor marker mucin 1 (MUC1). MB was attached to the distal terminus of the surface-bound aptamer.

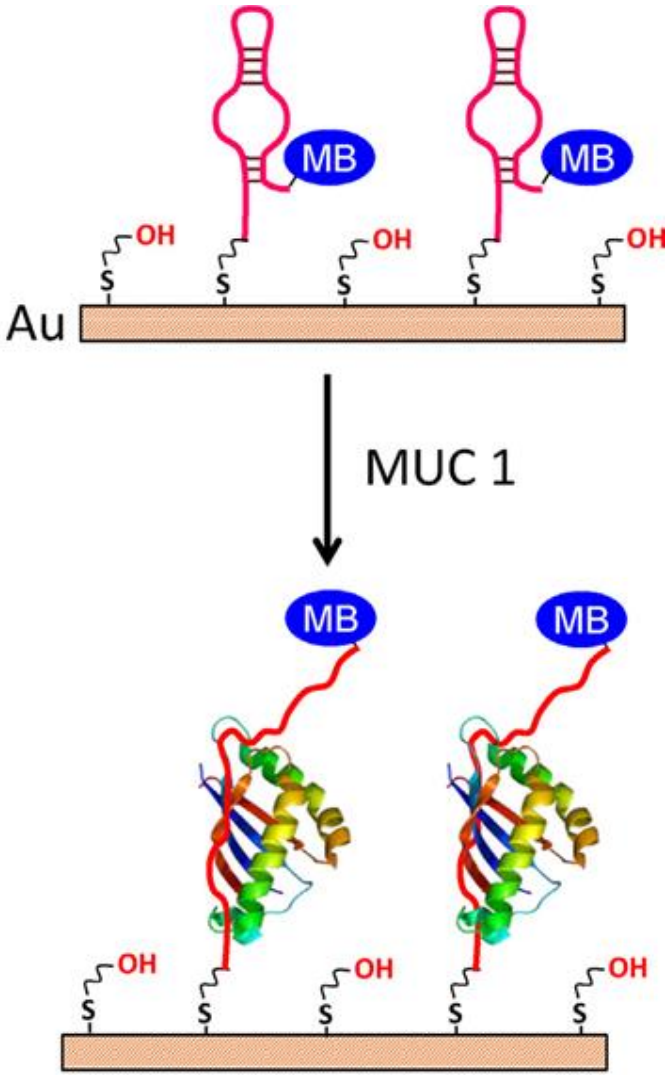

Figure 1.6. Possible conformational change of MB-anti-MUC1-aptamer (immobilized on gold electrode) upon binding MUC1.

Note. Reprinted with permission from Ma, F.; Ho, C.; Cheng, A. K. H.; Yu, H.-Z. Immobilization of Redox-Labeled Hairpin DNA Aptamers on Gold: Electrochemical Quantitation of Epithelial Tumor Marker Mucin 1. *Electrochim. Acta* 2013, *110*, 139–145. Copyright 2013 Elsevier.

Upon analyte binding, the conformation of the MB-labeled aptamer undergoes a conformational change, which pushes attached MB molecules further away from the electrode than the folded DNA. This conformational change contributes to a decrease of the electrochemical signal. Experimental results have shown that with increasing amounts of MUC1 the electrochemical signal keeps decreasing. The detection limit of this MB-labeled DNA sensor has been determined to be 50 nM with a response range up to 1.5 µM.[22]

Intercalation: Intercalation refers to the insertion of ligands into the stacked base pairs of DNA as shown in Figure 1.7. The interaction between these ligands and double-stranded DNA by spectroscopic and X-ray crystallographic methods has been studied in the 1980s.[23] In 1987 DNA structures were investigated via the reduction of purine and pyrimidine bases. Bard and his group published their research of metallointercalation agents in the presence of double-stranded DNA.[24] Tris(1,10-phenanthroline) cobalt (III) was employed in these experiments. It was found that $Co(phen)_3^{3+}$ can be used to probe the interaction with DNA upon the addition of DNA strands into an aqueous medium.

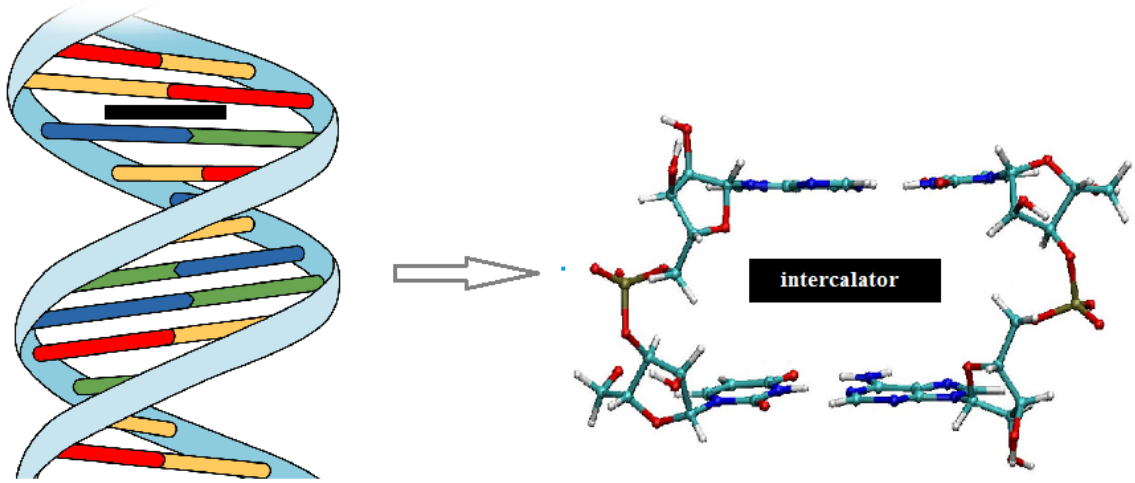

Figure 1.7. Intercalation of a planar molecule in double-stranded DNA. The intercalator is represented by the black rectangle.

As shown in Figure 1.7. (A), the addition of DNA strands caused the peak currents of the cyclic voltammetry (CV) waves for the reduction of $Co(phen)_3^{3+}$ to the reduced form and of the anodic peak on the reverse scan to decrease considerably. In all experiments the peak current I_p was proportional to the square root of the scan rate,

$v^{1/2}$, indicating that it is a diffusion-controlled process. In order to demonstrate that the lower peak current was caused by the binding of $Co(phen)_3^{3+}$ to the large, slowly diffusing DNA instead of the increase in solution viscosity, the researchers further performed similar experiments on a mixture of $Co(phen)_3^{3+}$ and $Mo(CN)_8^{4-}$. Different from $Co(phen)_3^{3+}$, the latter ligand $Mo(CN)_8^{4-}$ was negatively charged. It does not interact with the DNA because the phosphate backbone of DNA is also negatively charged. The CV results clearly showed the redox peaks of $Mo(CN)_8^{4-}$ stayed the same upon the addition of DNA while the redox peaks of $Co(phen)_3^{3+}$ were affected strongly by DNA as in the former experiments.

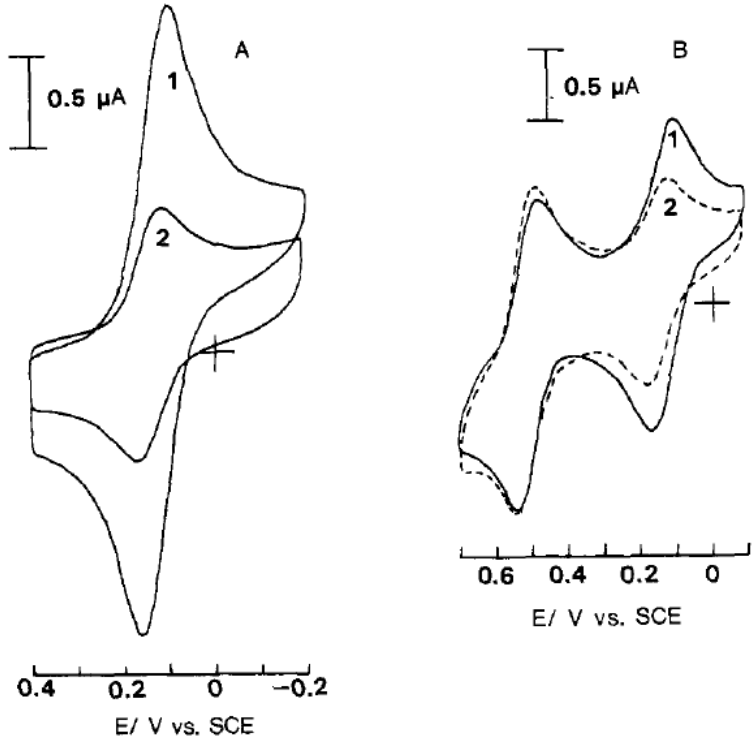

Figure 1.8. Cyclic voltammograms of (A) 0.12 mM $Co(phen)_3^{3+}$ (1) in the absence (E_{pc}=0.095 V, E_{pa}=0.160 V)and (2) in the presence of 5.3 mM nucleotide phosphate (E_{pc}=0.115 V, E_{pa}=0.175 V); (B) 0.10 mM $Co(phen)_3^{3+}$ and 0.01 mM $Mo(CN)_8^{4-}$ (1) in the absence and (2) in the presence of 4.7 mM nucleotide phosphate. Supporting electrolyte, 50 mM NaCl, 5 mM Tris, pH 7.1. Sweep rate, 100 mV/s. Glassy carbon as working electrode (0.07 cm^2). All potentials reported relative to saturated calomel electrode (SCE).

Note. Reprinted with permission from Carter, M. T.; Bard, A. J. Voltammetric Studies of the Interaction of Tris(1,10-Phenanthroline) cobalt(III) with DNA. *J. Am. Chem. Soc.* 1987, *109*, 7528–7530. Copyright 1987 American Chemical Society.

Further calculations have been done to compare the diffusion coefficient of $Co(phen)_3^{3+}$ by carrying out CV experiments with different ratios of DNA to $Co(phen)_3^{3+}$. The results showed the diffusion coefficient decreased 10-fold when the ratio went from 0 to 304.5. This demonstrated that the intercalation process can be characterized by simple electrochemical experiments and that redox intercalators can be used as probes for DNA structures.

In 1989, this group extended their work and published a paper on the interaction of other redox reporters with calf thymus DNA.[25] $Fe(phen)_3^{2+}$ (phen = 1,10-phenanthroline) was found to have similar behaviour as $Co(phen)_3^{3+}$ and also to have the ability to intercalate into a DNA duplex. The chemical structures of $Co(phen)_3^{3+}$ and $Fe(phen)_3^{2+}$ are shown below.

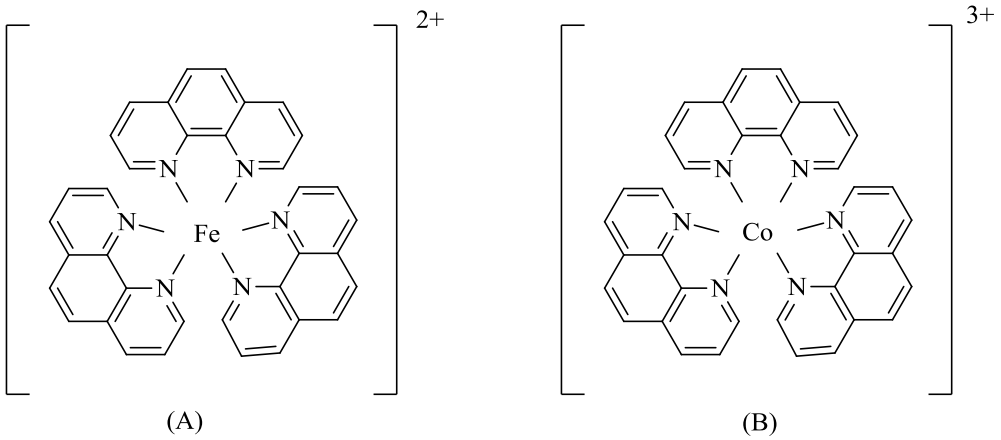

(A) (B)

Figure 1.9. Chemical structures of (A) $Fe(phen)_3^{2+}$ and (B) $Co(phen)_3^{3+}$ respectively.

More information such as binding site size, binding constant for the oxidized and reduced forms, and binding mode at different ionic strengths have been investigated by Pang and his co-workers in 1998.[26] Different from the afore-mentioned solution methods, they employed DNA-modified electrodes. $[Co(phen)_3]^{3+/2+}$ and $[Co(bpy)_3]^{3+/2+}$ were chosen as model compounds for the study. For $[Co(phen)_3]^{3+/2+}$, under high ionic strength conditions, the experimental results were inconsistent with the solution experiments, which indicated the binding mode between $[Co(phen)_3]^{3+/2+}$ and DNA strands is intercalation. The reduced form $[Co(phen)_3]^{2+}$ interacted with double-stranded DNA on a gold surface twice as strongly as the oxidized form $[Co(phen)_3]^{3+}$, which is

characteristic of intercalative interactions. When the ionic strength decreased to a certain value, the large negatively shifted formal potential suggested a change in the binding mode from intercalation to electrostatic interaction.

The interaction of double-stranded DNA with $[Co(bpy)_3]^{3+/2+}$ was also studied. Unlike $[Co(phen)_3]^{3+/2+}$, the domain interaction was always electrostatic. Pang's surface electrochemical experiment provided more detailed information about the binding process with smaller DNA samples than the solution method while they also pointing out drawbacks in the method such as tedious experimental steps and the time required for preparing DNA modified electrodes.

Electrostatic interaction: As shown in Figure 1.10, a double-stranded DNA is composed of base pairs and a sugar phosphate backbone. The phosphate groups bring negative charges to the DNA backbone, which attracts cations or compounds through electrostatic interaction. Taking advantage of this interaction, numerous studies have been done to exam DNA-modified surfaces, monitor hybridization of DNA strands, and detect biomarkers or small molecules.

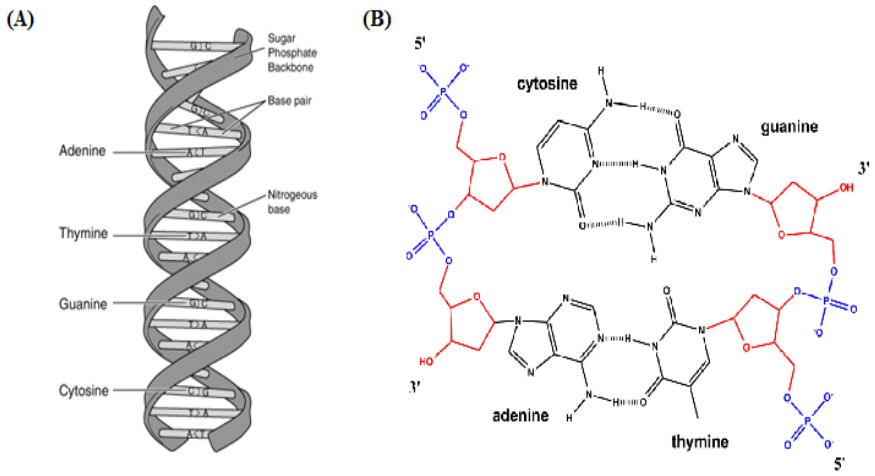

Figure 1.10. (A) The structure of a double helix DNA. Four kinds of bases have been labeled: Adenine (A), Thymine (T), Cytosine (C), and Guanine (G). (B) Base-pairing interaction of DNA. The ribose, phosphate group and aromatic bases are shown in red, blue, and black, respectively. Hydrogen bonding is shown by dashed lines.

$[Ru(NH_3)_6]^{3+}$, a redox active cation, has been widely used to examine DNA-modified surfaces. As a triply positively charged cation, it binds to the negatively charged DNA phosphate backbone through electrostatic interaction as mentioned above. This complex is known to be stable against hydrolysis at room temperature in water. The halftime for the substitution of NH_3 by H_2O in the dark being the order of days or even longer.[27,28] In 2003, our group has developed a simple, convenient, and reliable procedure to quantify the amount of surface-bound DNA based on the electrochemical response of $[Ru(NH_3)_6]^{3+}$, that is electrostatically bound to the DNA-modified surface .[29]

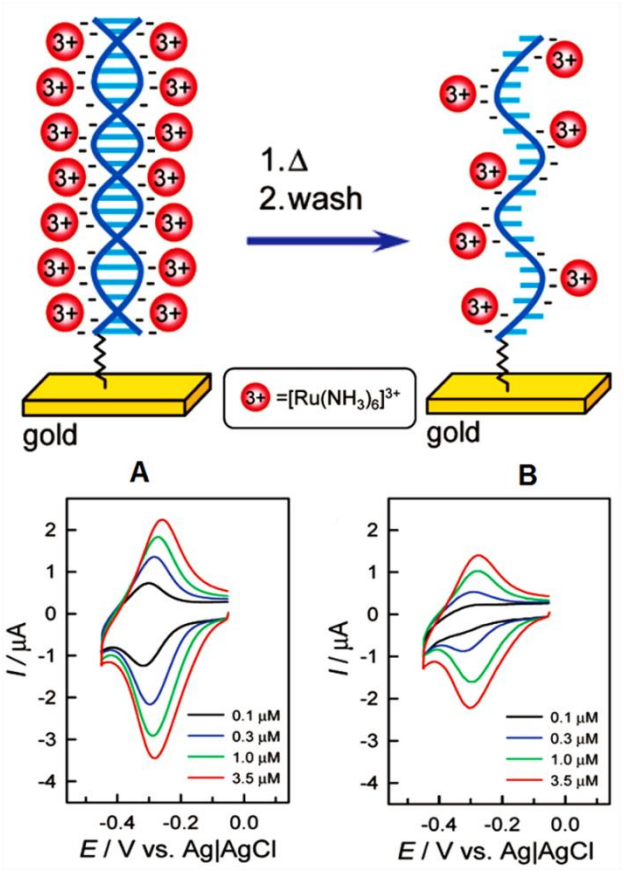

Figure 1.11. Pictorial representation and CV responses of $[Ru(NH_3)_6]^{3+}$ bound electrostatically to (A) double-stranded DNA, (B) single-stranded DNA-modified gold electrode in 10 mM Tris buffer (pH 7.4) in the presence of various concentrations of $[Ru(NH_3)_6]^{3+}$ as shown. The scan rate was 50 mV/s.

Note. Reprinted with permission from Yu, H.-Z.; Luo, C.-Y.; Sankar, C. G.; Sen, D. Voltammetric Procedure for Examining DNA-Modified Surfaces: Quantitation, Cationic Binding Activity, and Electron-Transfer Kinetics. *Anal. Chem.* 2003, *75*, 3902–3907. Copyright 2003 American Chemical Society.

As shown in Figure 1.11, they immobilized double-stranded DNA onto the gold surface and tested the CV responses in $[Ru(NH_3)_6]^{3+}$ solution at low ionic strength. An ion exchange equilibrium was reached between $[Ru(NH_3)_6]^{3+}$ and the native charge compensation ions (presumably Na^+) associated with the negatively charged DNA backbone. The surface concentration of $[Ru(NH_3)_6]^{3+}$ (Γ_{Ru}) reflected the surface density of the DNA strands. Taking into account the charge of the redox cation, the number of bases, and the number of electrons involved in the redox reaction, the surface density of DNA (Γ_{DNA}) can be determined.

The surface density of $[Ru(NH_3)_6]^{3+}$ can be calculated from

$$\mathrm{Q} = \mathrm{nFA}\Gamma_{Ru} \tag{1-15}$$

where Q is the charge obtained by integrating the cathodic peak of the cyclic voltammograms of the $[Ru(NH_3)_6]^{3+}$ redox reaction, n is the number of electrons involved in the redox reaction, and A is the surface area of the working electrode.

From the $[Ru(NH_3)_6]^{3+}$ adsorption isotherm, a saturation could be observed for both the single-stranded and the double-stranded DNA-modified electrode when the concentration of $[Ru(NH_3)_6]^{3+}$ reached 5 μM. Under the condition of saturation, the calculated Γ_{Ru} could be converted to Γ_{DNA} by applying the relationship

$$\Gamma_{DNA} = \Gamma_{Ru}(z/m)N_A \tag{1-16}$$

where m is the number of nucleotides in DNA, z is the charge of the redox cation $[Ru(NH_3)_6]^{3+}$, and N_A is Avogardro's number.

The validity of the afore-mentioned DNA quantification method relies on the following assumptions: (1) the redox cation $[Ru(NH_3)_6]^{3+}$ binds to the DNA strands only through electrostatic interactions; (2) the amount of trapped redox cations can be accurately determined; (3) the charge compensation of phosphate backbones is provided only by the redox cation $[Ru(NH_3)_6]^{3+}$; (4) the redox cation is electrochemically stable; and (5) every phosphate group is accessible for electrostatic binding.

The reliability of this DNA quantification method has been demonstrated by comparing the result with those obtained by chronocoulometry (CC), and radio-isotope labeling and reading method. Three kinds of DNA strands have been used in the experiment: unmodified single-stranded DNA, thiol labeled single-stranded DNA, and thiol labeled double stranded DNA. Both CV and CC methods showed similar results in calculating the DNA surface density within experimental uncertainties.[30] It is noticeable that the cathodic peak of the $[Ru(NH_3)_6]^{3+}$ CV scans was larger than the anodic peak. This is probably due to the smaller binding constant of $[Ru(NH_3)_6]^{2+}$ comparing to $[Ru(NH_3)_6]^{3+}$, which probably also results in a decrease of the redox peaks during repeated CV scans. Therefore, in order to get DNA densities precisely, it is critical to carefully choose the experimental conditions. Taking the charge under the first CV scan at a high scan rate (usually 500 mV/s) helps to provide a more accurate result. In addition, the adsorption isotherm showed that 5-10 μM $[Ru(NH_3)_6]^{3+}$ is sufficient to saturate the DNA-modified gold surface within 15 min. Under those conditions, the influence of the solution diffusion process could be neglected by running the experiment at a high scan rate (500 mV/s).

Table 1.1. Comparison of different electrochemical quantitation of DNA surface densities on DNA-modified gold electrode with radioactivity measurements and literature values.

	Unmodified ssDNA ($\times 10^{12}$ molecules/cm^2)	HS-ssDNA ($\times 10^{12}$ molecules/cm^2)	HS-dsDNA[c] ($\times 10^{12}$ molecules/cm^2)
CV[a]	0.11 ± 0.04	19.9 ± 2.7	5.3 ± 1.2
CC[a]	N/A	19.7 ± 2.2	5.4 ± 1.3
CC[b]	0.80 ± 0.09	22.1 ± 3.2	5.8 ± 1.7
^{32}P-radiolabeling	N/A	23.0 ± 0.9	N/A
Literature		5.2 ± 0.8 [8a,8e]	7.2 [5b]
		11 ± 0.2 [8b]	4.6 ± 0.6 [10]
		7.2 [12]	2.8 ± 0.6 [8b]
		50 [8c]	

[a] Performed with 3.5 μM $[Ru(NH_3)_6]^{3+}$.
[b] Measured in 50 μM $[Ru(NH_3)_6]^{3+}$.
[c] Prepared by adsorption of pre-hybridized samples on gold; the values refer to the number of double helices.

Note. Reprinted with permission from Ge, B.; Huang, Y.-C.; Sen, D.; Yu, H.-Z. Electrochemical Investigation of DNA-Modified Surfaces: From Quantitation Methods to Experimental Conditions. *J. Electroanal. Chem.* **2007**, *602*, 156–162. Copyright 2007 Elsevier.

The ion-exchange binding of non-electroactive ions, such as Ca^{2+}, Mg^{2+}, and K^+ ,to the DNA-modified surface has been studied through a simple protocol utilizing the electrostatic interaction between $[Ru(NH_3)_6]^{3+}$ and DNA.[31] As shown in Figure 1.11, after incubation with 5 μM $[Ru(NH_3)_6]^{3+}$, the DNA-modified gold electrodes were further exposed to different concentrations of these non-electroactive metal cations. The CV

responses of pre-bound $[Ru(NH_3)_6]^{3+}$ exhibited significant changes such as a decrease in integrated charge and formal potential shift.

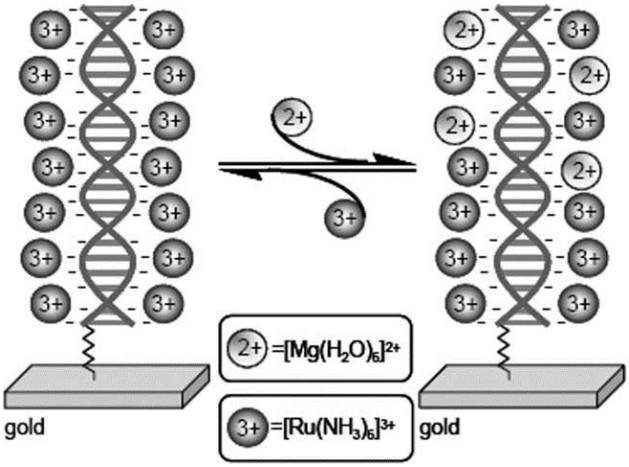

Figure 1.12. Schematic illustration of the ion-exchange binding process of Mg^{2+} (in the form of $[Mg(H_2O)_6]^{2+}$)to a double-stranded DNA modified gold electrode that has been previously incubated with $[Ru(NH_3)_6]^{3+}$.

Note. Reprinted with permission from Su, L.; Sen, D.; Yu, H.-Z. Voltammetric Study of the Ion-Exchange Binding of Non-Electroactive Metal Cations to DNA-Modified Surfaces. *Analyst* 2006, *131*, 317–322. Copyright 2006 Royal Society of Chemistry.

The divalent cations showed a stronger binding ability to the $[Ru(NH_3)_6]^{3+}$ pre-saturated thiolated DNA helixes monolayers on gold than the monovalent cation K^+. The formal potential shift was triggered by 10 μM Mg^{2+} and 100 μM Ca^{2+} while the threshold concentration of K^+ was 5 mM. The binding constants (*K*) were calculated to be 6.7 ± 0.5 × 10^4 M^{-1} and 3.8 ± 0.5 ×10^4 M^{-1} for Mg^{2+} and Ca^{2+}, respectively. Compared to the multiply charged $[Ru(NH_3)_6]^{3+}$ (K = 2.0 ± 0.5 ×10^6 M^{-1}), the binding between Ca^{2+} , Mg^{2+} to DNA is much weaker.

After these fundamental studies of $[Ru(NH_3)_6]^{3+}$ and thiolated DNA monolayers on gold electrodes, a label-free aptamer-based biosensor was proposed for detecting lysozyme.[32] Aptamers are small single-stranded nucleic acids that fold into a well-defined three dimensional structure. They have a high and specific affinity to their target molecules.[33] In this case, thiolated lysozyme aptamers were immobilized onto a gold electrode through strong Au-S bonds to form monolayers. Due to the positive charge of lysozyme, the negatively charged aptamer would be partly neutralized after binding, resulting in a decrease of the amount of electrostatically bound $[Ru(NH_3)_6]^{3+}$. Therefore,

the electrochemical response of $[Ru(NH_3)_6]^{3+}$ would decrease accompanied by an increasing concentration of lysozyme.

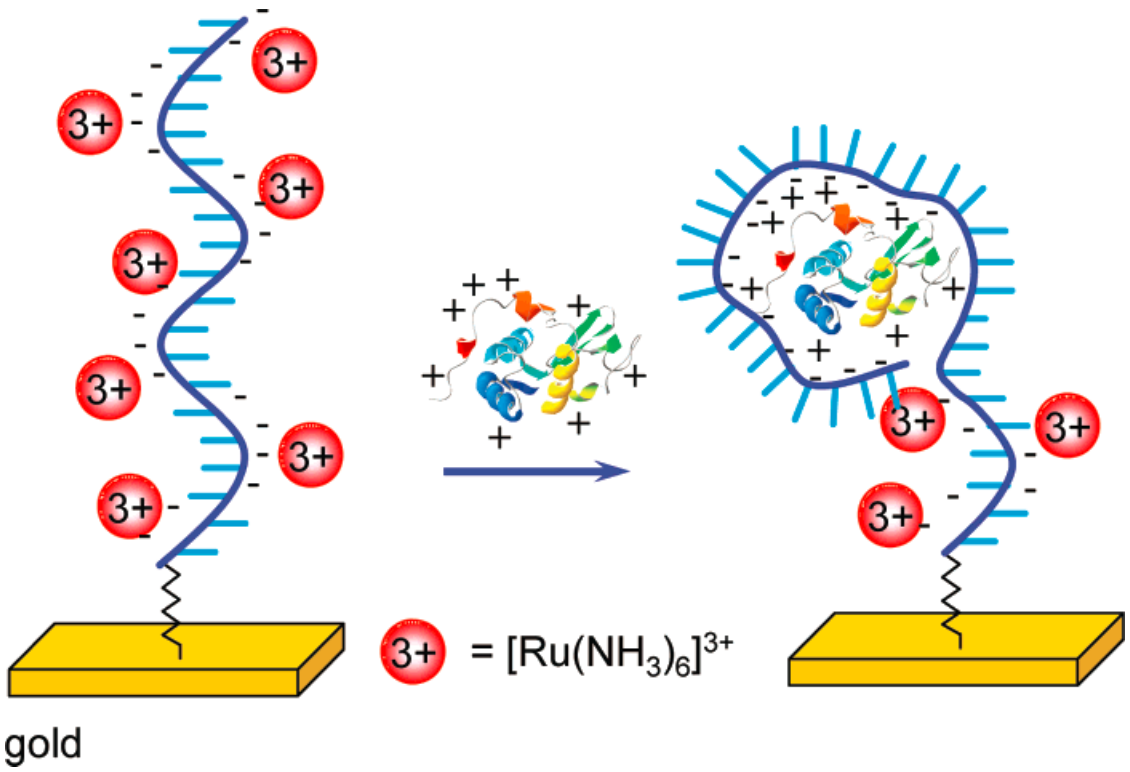

Figure 1.13. Schematical illustration of the working principle of a proposed aptasensor. The lysozyme aptamer undergoes a conformational change after binding with lysozyme. The resulting neutralization reduces the electrostatic interaction between $[Ru(NH_3)_6]^{3+}$ and DNA monolayers.

Note. Reprinted with permission from Cheng, A. K. H.; Ge, B.; Yu, H.-Z. Aptamer-Based Biosensors for Label-Free Voltammetric Detection of Lysozyme. *Anal. Chem.* 2007, *79*, 5158–5164. Copyright 2007 American Chemical Society.

This DNA based sensor exhibited an excellent specificity towards lysozyme rather than cytochrome *c*, which has a similar size and also is positively charged under experimental conditions. Because a very high DNA surface density would hinder the folding of aptamers due to spatial restriction, while a very low DNA surface density would be strongly influenced by the diffusion-controlled process, the suitable DNA surface density had to be optimized to reach the highest relative signal change. As for the detection limit, this aptasensor was proved to be capable of detecting physiological concentrations of lysozyme (between 0.5 and 50 μg/mL) in a sample.

1.2. Immunoassay

One of the most selective reagents provided by nature is called antibody. As an important component of the immune defense system, antibodies are generated by specific organs within weeks after injecting a foreign species, which is usually called antigen. Due to its excellent ability of specific recognition of binding to the target, antibodies are widely used in chemistry and biochemistry. As one of the most active research tools, immunoassay techniques have been drawing attention in several paramount fields, such as diagnosis[34], drug discovery[35], food quality testing[36], and environmental safety monitoring[37]. By taking advantage of the specific recognition between antibody and antigen, the immunoassay test provides an extraordinarily selective and sensitive way to quantitate the target of interest.[38]

Enzyme-linked immunosorbent assay (ELISA), the most widely used and trustable immunoassay approach for quantitative protein detection, was invented half a century ago.[39] This method allows us to detect and quantify substances such as antibodies, peptides, and hormones by immobilizing the capture antibodies onto a solid surface which binds specific antigens. Detection antibodies that are tethered with an enzyme for signal enhancement are added to form a sandwich-like structure.[40] Horseradish peroxidase (HRP) is a commonly used enzyme in ELISA which catalyzes the reaction between 3,3',5,5'-tetramethylbenzidine (TMB) and H_2O_2; the blue colored product is quantitated by UV/Vis spectrometry.[41]

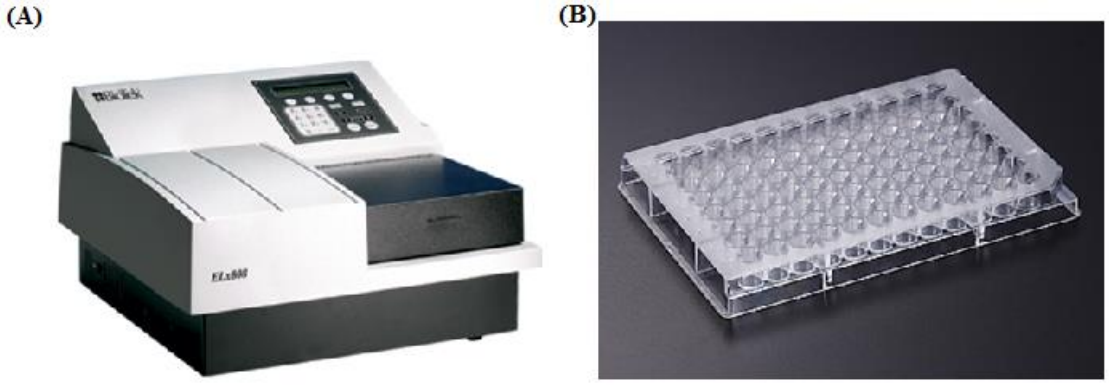

Figure 1.14. Commercially used ELISA equipment: (A) ELISA plate reader and (B) a 96-well ELISA plate.

1.2.1. Types of immunoassay

Depending on the availability of antibodies as well as the target of interest, immunoassays can be generally divided into three different types: direct assay, sandwich assay, and competitive assay.

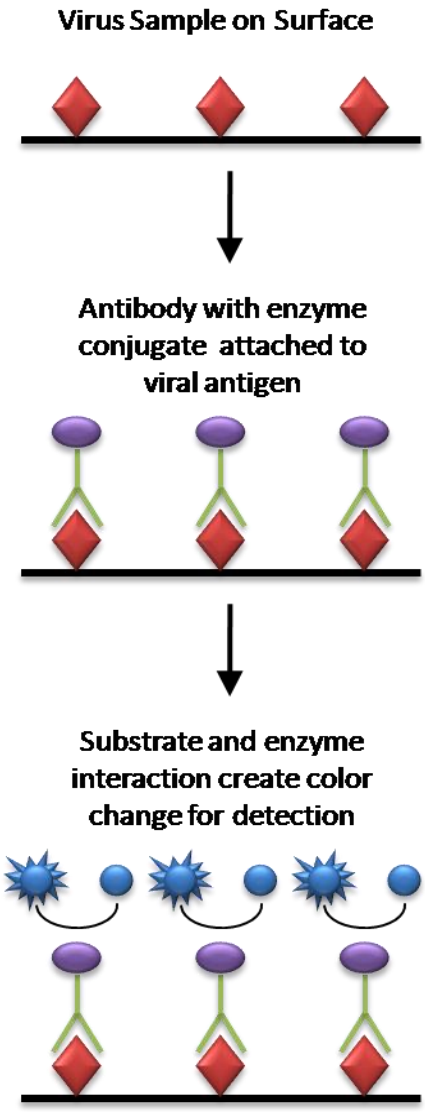

Figure 1.15. Pictorial description of the working principle of a direct assay. The substrate is shown as a black line. Antibody-enzyme conjugate has been used as example.

Direct immunoassays. In direct assay, the sample that contains target antigens is directly immobilized onto the substrate surface through physical adsorption or chemical bonds. After blocking the surface with nonreactive protein (such as bovine serum albumin, BSA), the primary antibody that specifically binds to the target antigens will be added and incubated for a long time. The primary antibody is tethered with an enzyme or other dye molecules depending on the desired readout method. The excess primary antibodies are washed away by buffers so only the antibodies that bind to antigen are left and produce a signal. A stronger signal indicates that more antibodies have been attached to the surface, which means more antigens are present in the sample. In this way, the amount of target antigens can be quantified.

It should be pointed out that there is a major drawback of direct immunoassays. As shown above, the sample is immobilized onto the surface nonspecifically, which results in the immobilization of other unwanted proteins in serum or other body fluids to the substrate through physisorption. The small amount of antigens in the sample needs to compete with other proteins when binding to the surface, leading to a low signal intensity. This disadvantage limits the application of direct immunoassays to real sample testing.

Sandwich-format immunoassays. The sandwich type immunoassay is the most commonly used immunoassay in real sample testing in hospitals. Compare to the direct assay, a layer of capture antibodies is firstly immobilized onto the substrate surface instead of antigens. The following steps are similar to the direct assay: nonreacted proteins are added to further block the surface, followed by adding samples that contain the target antigens. In this way, only the target antigens can be attached to the surface through antibody-antigen binding while other interferences are later washed away by buffers. Finally, enzyme-linked detection antibodies are added and bind to antigen forming a “sandwich” structure. The capture antibody and the detection antibody both are capable to recognize the target antigen and bind to different sites. After the signal read-out step, target proteins can be quantified.

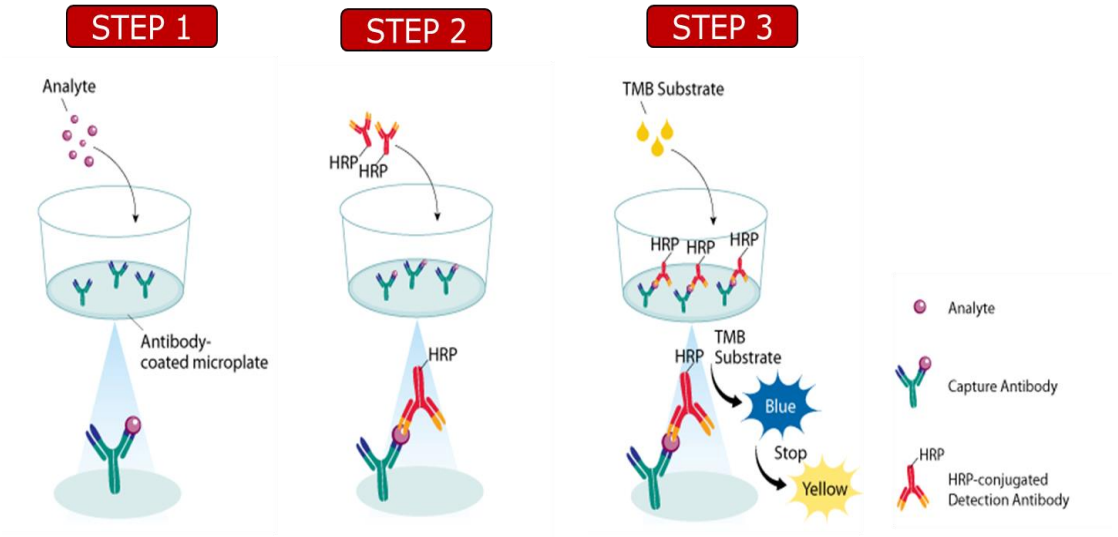

Figure 1.16. Pictorial illustration of the sandwich assay working principle. One of the 96 wells of an ELISA plate was used as representative. Here only one of many detection antibody labeling methods is shown, and labeled by HRP.

In order to perform a sandwich assay, more steps are needed compare to the direct assay. In addition, two different antibodies need to be harvested for each antigen, which causes some difficulties and more work for antibody generation.

Competitive immunoassays. The word “competitive” refers to the binding competition between the antibodies in solution and antibodies on the surface to the immobilized antigens. Unlike the afore-mentioned methods, the surface is initially modified by the target antigens and blocked with unreacted protein. Later the enzyme-labeled antibodies are added and bind to the surface through antibody-antigen recognition. The next step is to add samples that contain the target antigens. Therefore, some pre-bound antibodies will leave the surface antigen and bind to the antigen in sample solution and be washed off during the buffer washing step. Only the surface-bound antibodies can produce a signal. In other words, the more antigens in the sample solution, the more antibodies will leave the surface, the less antibodies will be left on the surface. As a result, the higher the amount of antigens contained in the sample, the lower will be the signal obtained.

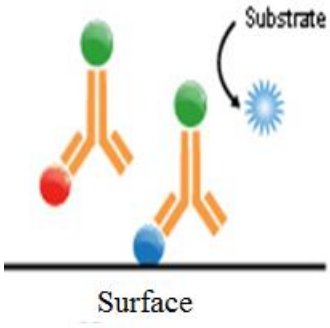

Figure 1.17. Pictorial illustration of working principles of a competitive assay. The blue circle and the red circle represent surface-bound antigen and antigen in solution, respectively. The green dot represents the enzyme that is conjugated with the antibody.

1.2.2. Signal enhancement strategies

In order to quantify the trace amount of target of interest in serum or other human fluids, signal enhancement is critical for reaching a low detection limit. Researchers have proposed several strategies to achieve that goal.

In ELISA, the detection antibody is labeled with enzymes such as HRP. Antibodies can recognize the target of interest while enzymes are used to provide measurability. As mentioned before, HRP catalyzes the reaction between 3,3',5,5'-tetramethylbenzidine (TMB) and H_2O_2; the blue colored product is quantitated by UV/Vis spectrometry, the typical readout for ELISA tests.

The most common method used for labeling the detection antibodies with HRP is treatment with periodate. Sodium periodate can oxidize the polysaccharide residues in HRP to generate aldehyde groups that can conjugate with antibodies by reacting with amino groups. However, in order to protect the enzyme activity, the reacting time should be less than 30 minutes. Also, this reaction must be done in the dark to prevent the breakdown of periodate groups.[42]

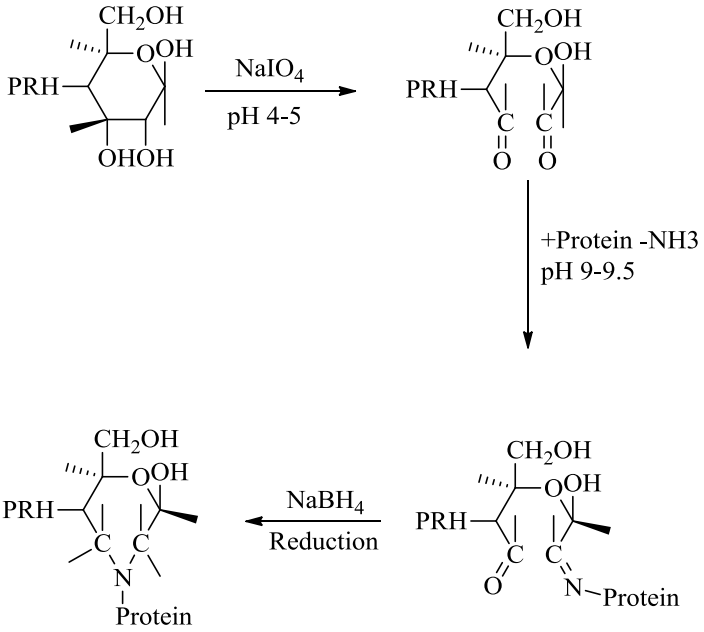

Figure 1.18. Principles of conjugating antibodies with HRP.

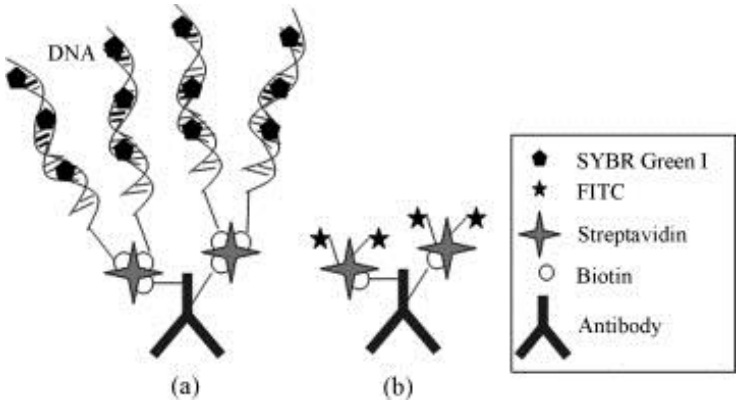

Figure 1.19. Pictorial illustration of the new antibody labeling strategy and comparison with the traditional labeling method. (a) Biotin-labeled long-chain DNA carrying a large number of fluorescent DNA binders SYBR Green I linked to biotinylated antibody via streptavidin. (b) Traditional approach of using FITC-streptavidin to label the antibody.

Note. Reprinted with permission from Zhu, S.; Zhang, Q.; Guo, L. H. Part-per-Trillion Level Detection of Estradiol by Competitive Fluorescence Immunoassay Using DNA/dye Conjugate as Antibody Multiple Labels. *Anal. Chim. Acta* 2008, *624*, 141–146. Copyright 2008 Elsevier.

DNA-dye molecule conjugates: Zhu and his coworkers explored a new labeling strategy for fluorescent signal enhancement.[43] Instead of simply labeling the detection antibody with fluorescent dye molecules, the utilization of a 219 base-pair DNA with the

fluorescent DNA binder SYBR Green I produced a more than six-fold increase in signal intensity.

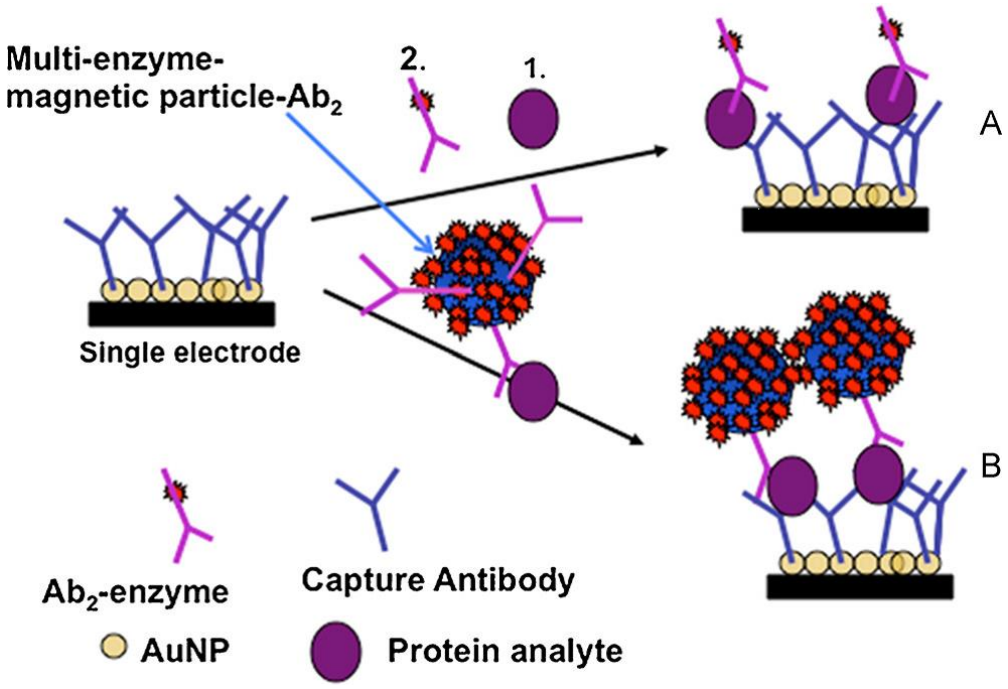

Figure 1.20. Alternative strategies for electrochemical signal amplification featuring gold nanoparticle surfaces with capture antibodies immobilized: (A) immunosensor after incubation with target protein and a traditional single-enzyme-labeled detection antibody; (B) thousands of HRP are attached onto MP and the MP-Ab2-HRP-analyte conjugates are trapped by capture antibodies on the electrode. Electrochemical signals are generated by injecting a solution of mediator and hydrogen peroxide.

Note. Reprinted with permission from Chikkaveeraiah, B. V.; Mani, V.; Patel, V.; Gutkind, J. S.; Rusling, J. F. Microfluidic Electrochemical Immunoarray for Ultrasensitive Detection of Two Cancer Biomarker Proteins in Serum. *Biosens. Bioelectron.* 2011, *26*, 4477–4483. Copyright 2011 Elsevier.

This approach allowed the binding of a large amount of dye molecules to the long DNA chain and also, because of the nature of this dye molecule, it only binds in situ to the oligonucleotide through specific binding interaction. The unbound DNA strands can't emit fluorescence, so that the measurement can be performed with a washing step.[44] By taking advantage of a rather long double-stranded DNA, the detection limit improved 10-

fold and reached the part-per-trillion level for the detection of estradiol compared to the traditional fluorescein-labeled antibody approach.

Multi-enzyme magnetic particle-antibody conjugates: Another signal amplification strategy was proposed by Chikkaveeraiah and his colleagues. As shown in Figure 1.20, the detection antibodies and HRP labels were conjugated onto superparamagnetic particles (MPs).[45]

Mps were conjugated with about 90,000 antibodies and 200,000 HRP, which helped to provide a high sensitivity (sub-pg mL^{-1} levels). What's more, the combination of microfluidic design, detection of two cancer biomarkers in serum, prostate specific antigen (PSA) and interleukin-6 (IL-6) simultaneously has been achieved.

DNA hybridization chain reaction: Recently a novel signal enhancement strategy based on the formation of DNAzyme concatamers stimulated by the DNA hybridization chain reaction (HCR) has been proposed by Hou and his colleagues.[46] DNA concatamer refers to a linear polymeric structure that formed by self-association of short DNA fragments via specific interactions.[47] The working principle is shown in Figure 1.21.

DNA concatamers were formed by the hybridization chain reaction between the initiator DNA strand and two auxiliary DNA strands. After that, numbers of DNAzymes were generated in the presence of hemin, which catalyzed the reaction of H_2O_2 with 4-chloro-1-naphthol. The resulting product benzo-4-chlorohex-adienone is insoluble and precipitated on the electrode surface, resulting in the hindrance of electron transfer of the redox probe in solution to the electrode. The signals were recorded by electrochemical impedance spectroscopy, reflecting the amount of the target that immobilized onto the surface by the sandwich structure. This resulted in a large improvement of the detection range for the model protein carcinoembryonic antigen (CEA) from 1.0 pg mL^{-1} to 20 ng mL^{-1} with a detection limit of 0.42 pg mL^{-1}.

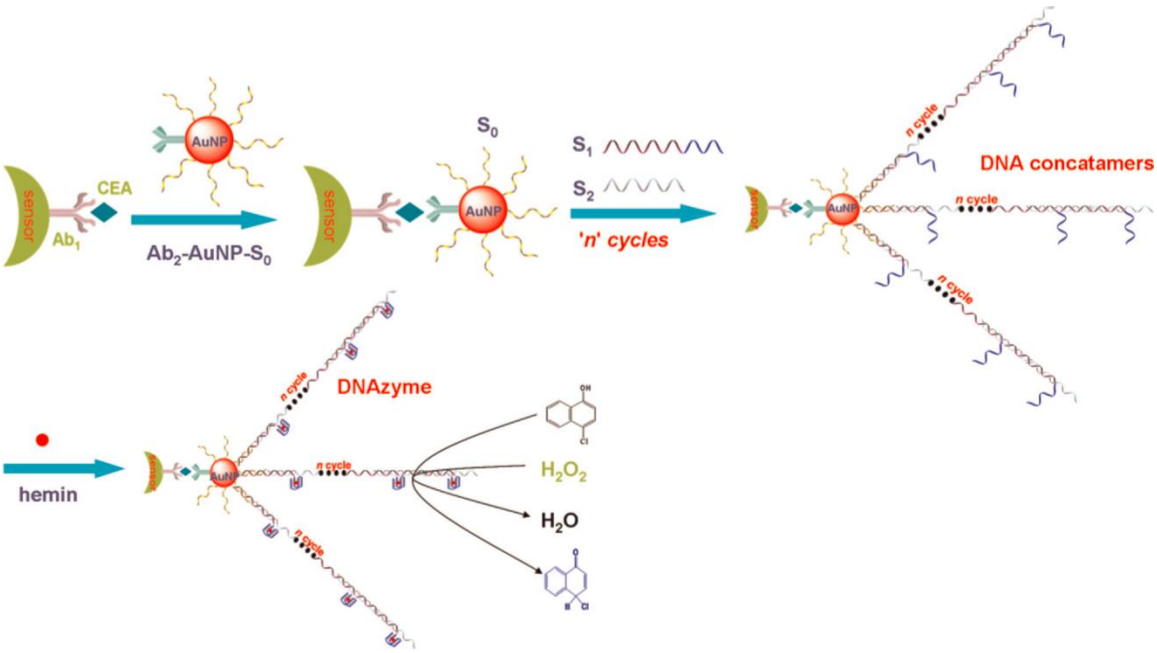

Figure 1.21. Schematic illustration of DNA hybridization chain reaction triggered formation of DNAzyme concatamers for signal amplification of the impedimetric immunosensor. Gold nanoparticles were modified with initiator strands (S_0). After the sandwich structure was formed, two auxiliary single-stranded DNAs (S_1, S_2) were added for the formation of DNA concatamers. In the presence of hemin, DNAzyme was formed and catalyzed the reaction between H_2O_2 and 4-chloro-1-naphthol.

Note. Reprinted with permission from Hou, L.; Wu, X.; Chen, G.; Yang, H.; Lu, M.; Tang, D. HCR-Stimulated Formation of DNAzyme Concatamers on Gold Nanoparticle for Ultrasensitive Impedimetric Immunoassay. *Biosens. Bioelectron.* 2015, *68*, 487–493. Copyright 2015 Elsevier.

1.2.3. Immunoassay with electrochemical readout

Although ELISA has been commercially used as the standard method for protein detection, the relatively expensive test kits as well as the large, non-portable equipment still hinder the application of ELISA in point of care (POC) diagnostics.[48] In order to address this issue, researchers have been trying to combine other readout methods with immunoassay to make a smaller, portable device. Therefore, electrochemical immunoassay has been developed to further merge the benefits from both sides while still providing a reliable results.

Compared to other signaling techniques, such as radioimmunoassay, colorimetric assay, and fluorescence immunoassay, electrochemical immunosensors exhibit the merits of cost effectiveness, good portability as well as excellent sensitivity.[13]

Zhang and his coworkers proposed a highly sensitive electrochemical detection method for immunospecies by utilizing ferrocene-labeled antibodies.[49] Human IgG has been used as a model analyte.

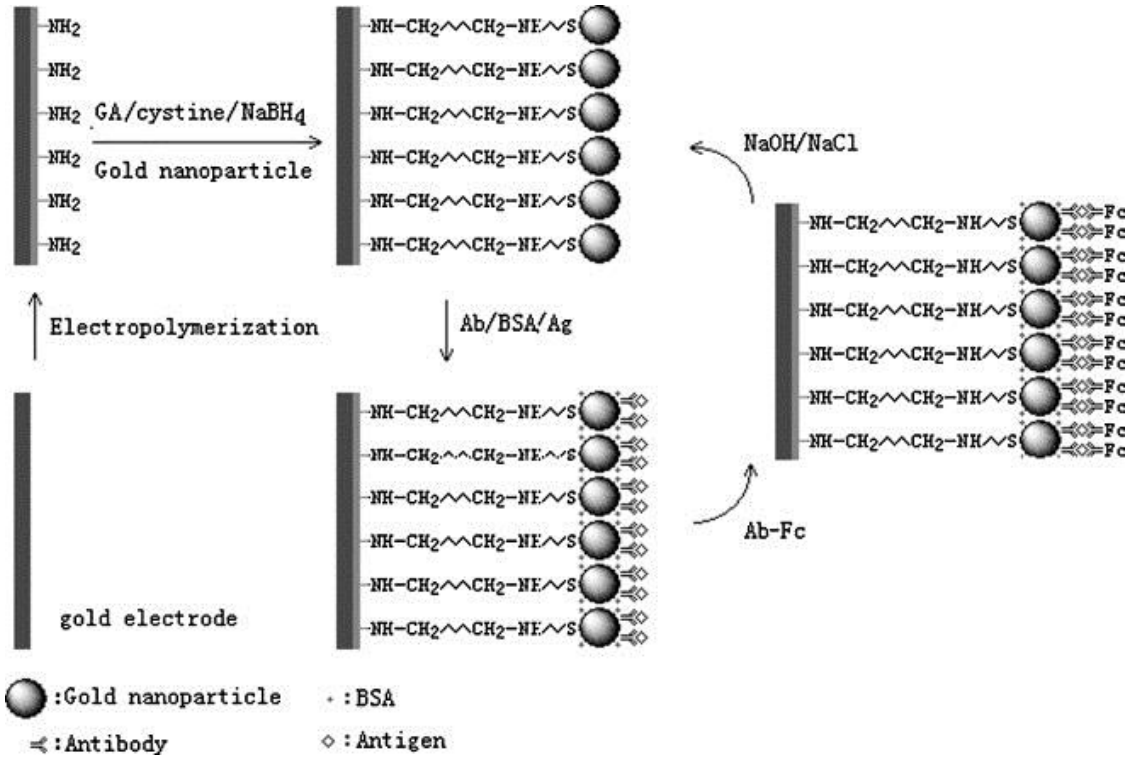

Figure 1.22. Schematic illustration of the fabrication of the sensing interface.

Note. Reprinted with permission from Zhang, S.; Zheng, F.; Wu, Z.; Shen, G.; Yu, R. Highly Sensitive Electrochemical Detection of Immunospecies Based on Combination of Fc Label and PPD Film/gold Nanoparticle Amplification. *Biosens. Bioelectron.* 2008, *24*, 129–135. Copyright 2008 Elsevier.

As shown in the figure above, the authors first introduced amino groups onto a gold electrode by electropolymerization. A gold nanoparticle monolayer was later on assembled onto the electrode by using glutaradehyde as cross-linker. After that, the capture antibodies can be self-assembled onto the surface via the strong affinity between gold nanoparticles and amino groups. The ferrocene-labeled detection antibody can be attached to the electrode surface through antibody-antigen recognition. This

detection system provides a wide linear range from 25 to 1000 pg/ mL with a detection limit of 10 pg/mL. This proposed system bear the merits of high selectivity and stability.

Signal amplification for electrochemical immunosensors is crucial for the purpose of early detection of disease-related protein in a patient's serum sample when present at an ultralow level.[50] Therefore, several strategies for signal enhancement have been reported other than simply labeling the antibodies with redox-active tags,[48] among which the use of enzymes to amplify the throughput signal is the most notable strategy.[51,52]

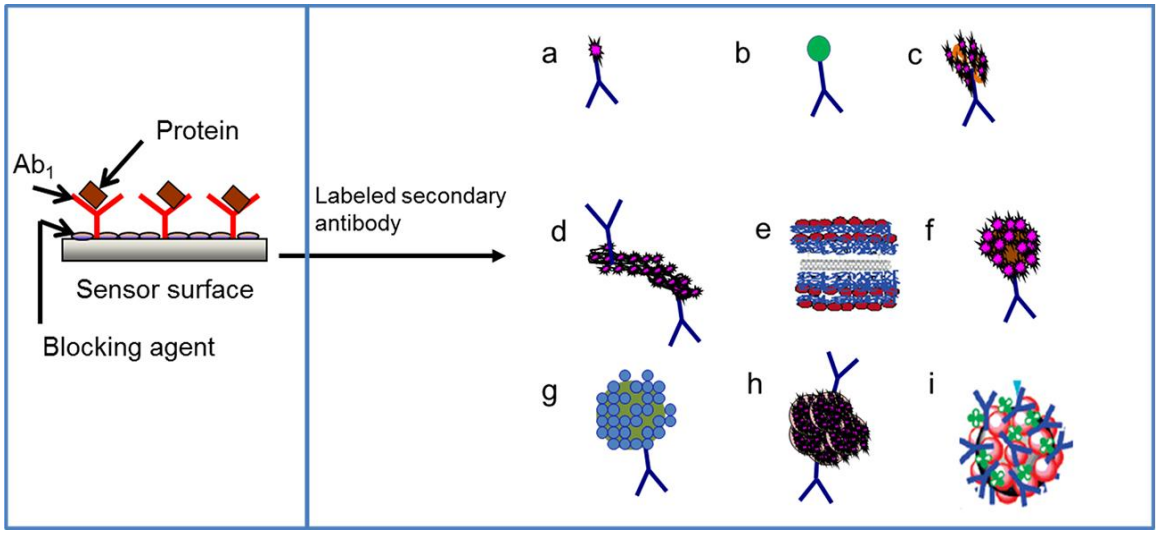

Figure 1.23. Different labeling strategies for singnal enhancement in electrochemical immunosensors. After the surface-bound capture antibody binds to the target protein, the labeled detection antibody binds to the target protein forming a sandwich structure. An electrochemical signal is generated using a substrate suitable for the electroactive species. (a) Ab2-enzyme, (b) Ab2-nanoparticle, (c) Ab2-biotin-streptavidin-enzyme, (d) Ab2-CNT-enzyme, (e) CNT-(PDDA-AP)$_4$-PDDA-PSS tag, (f) multienzyme-Ab2-nanoparticle, (g) Ab2-nanoparticle-Qdots, (h) Ab2-MB-multienzyme clusters, and (i) MB-AuNP-Ab2-multienzyme.

Note. Reprinted with permission from Chikkaveeraiah, B. V.; Bhirde, A. A.; Morgan, N. Y.; Eden, H. S.; Chen, X. Electrochemical Immunosensors for Detection of Cancer Protein Biomarkers. *ACS Nano* 2012, *6*, 6546–6561. Copyright 2012 American Chemical Society.

However, the protein enzyme-labelling process is not easily achieved, and this process may influence the biospecific sites and the biological activity of the enzyme.[53] As a result, label-free immunosensors have pronounced advantages in simple

fabrication, easy handling, and low cost due to the avoidance of the fussy labeling process.[54]

For the purpose of developing label-free immunoassays with better sensitivity and easier preparation, new materials have been fabricated and tested. The wide application of carbon-based materials has attracted much attention.[55] Liu and his coworkers developed a strategy by using reduced graphene oxide (rGO). [56]

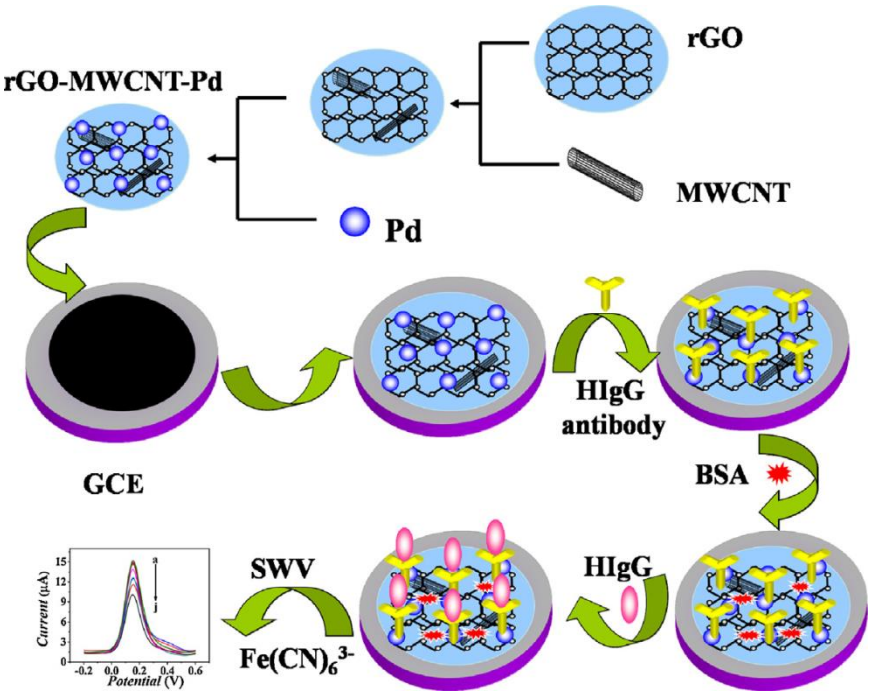

Figure 1.24. Illustration of stepwise electrode modification and fabrication of the electrochemical immunoassay. rGO-MWCNT-Pd nanocomposite was used basal material.

Note. Reprinted with permission from Liu, L.; Li, Y.; Tian, L.; Guo, T.; Cao, W.; Wei, Q. A Label-Free Voltammetric Immunoassay Based on 3D-Structured rGO–MWCNT–Pd for Detection of Human Immunoglobulin G. *Sensors Actuators B Chem.* 2015, *211*, 170–176. Copyright 2015 Elsevier.

rGO has been reported to have good conductivity for electrons.[57] With the help of hydrogen bonding, π-π stacking, and van der Waals forces, multiwalled carbon nanotubes (MWCNTs) can be inserted into grapheme sheet. The addition of MWCNTs helped to increase surface area and also inhibited the aggregation of graphene sheets and some weak interactions such as π-π stacking, hydrogen bonding, and Vander Waals forces.[58] Pd nanoparticles (Pd NPs) were induced to facilitate electron transfer

from the redox center of the protein to the electrode surface.[59] The fabricated rGO-MWCNT-Pd nanocomposite was used to amplify the electrochemical response and improve the sensitivity of the immunosensor. A solution of $K_3[Fe(CN_6)]$/PBS was used for electrochemical measurements. The binding of target to the electrode surface through antibody-antigen recognition restricted the current response and contributed to a decrease in signal. In this way, no label was needed for labeling antibodies.

The proposed immunosensor was used to quantify the amount of human immunoglobulin G (HIgG) and reached a rather low detection limit of 3.3 pg/mL, a wide linear range from 0.01-25 ng/mL and was accompanied by high stability, reproducibility and good selectivity.

1.3. Human chorionic gonadotropin: detection and quantitation

1.3.1. Biochemistry of hCG

Human chorionic gonadotropin (hCG) is a 237 aminoacid glycoprotein hormone produced by conceptus throughout the entire pregnancy period. It is a heterodimer consisting of two subunits, α and β, which attach to each other non-covalently by hydrophobic and ionic interaction.[60]

hCG is one of four glycoprotein hormones, which also include luteinizing hormone (LH), follicle stimulating hormone (FSH), and thyroid stimulating hormone (TSH). The α-subunit of hCG is identical to that of the other three hormones while the β-subunit is unique to hCG due to the fact that it confers the biological and immunologic specificity.[61] The hCG α-subunit contains 92 amino acids linked by five disulfide bridges. Two N-linked oligosaccharide side chains are attached at amino acid residue 52 and 78 of the hCGα-subunit. While the β-subunit of hCG is composed of 145 amino acids linked by six disulfide bridges. It also has two N-linked oligosaccharide side chains attached to residues 13 and 30. Four O-linked oligosaccharide units are located at the unique proline- and serin-rich C-terminal extension (residues 122 to 145).[62]

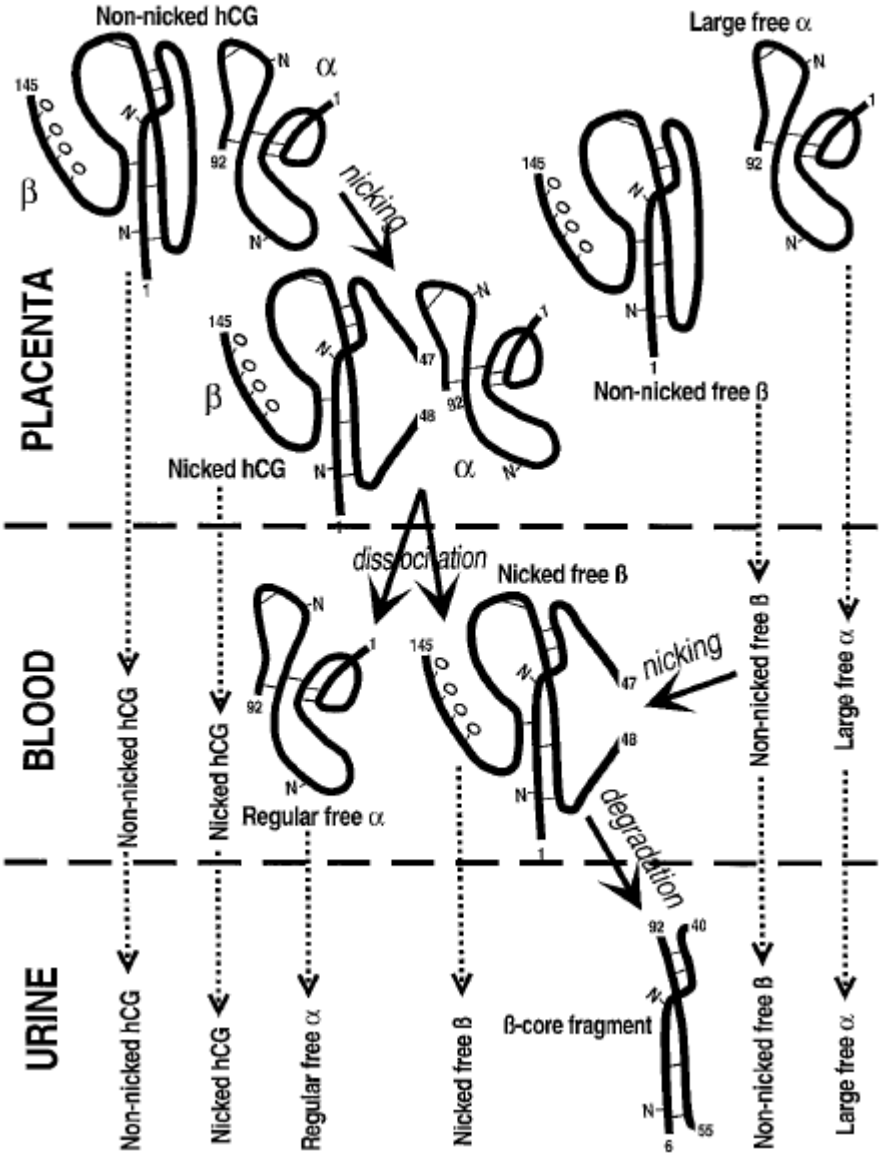

Figure 1.25. Illustration of hCG structures in the placenta, blood, and urine. The thick black lines represent the polypeptide chain. Numbers refer to the amino acid numbers in the chain. Thin lines represent disulfide linkages.

Note. Reprinted with permission from Cole, L. A. Immunoassay of Human Chorionic Gonadotropin, Its Free Subunits, and Metabolites. *Clin. Chem.* 1997, *43*, 2233–2243. Copyright 1997 American Association for Clinical Chemistry.

In circulation, hCG exits mainly in the form of the intact hormone (α-β dimer) with only a small percentage of free α-subunit and free β-subunit. However in urine, many fractions exist such as free α-subunit, free β-subunit, hCG dimer, hCG β-core fragment,

and nicked hCG, which has a single cleavage between residues 47 and 48 of the β-subunit peptide..[63]

1.3.2. Clinical importance of hCG measurement

hCG has significant biological functions. After implantation, the trophoblast that surrounds the blastocyst starts to release hCG into the maternal circulation. The increasing concentration of hCG stimulates the corpus luteum to secrete progesterone during the first trimester.[63]

What's more, hCG is also an important biomarker that has been used for a variety of clinical diagnoses such as pregnancy, pregnancy-related disorder, and gynecological cancers.[64] In general, the last menstrual bleeding is considered as the onset of pregnancy; the concentration of biologically active hCG (non nicked hCG) in serum and urine exbibits a dramatical exponential increase every 48-72 hours, reaches the peak value during the 9th to 12th weeks of gestation, experiences a decrease from the 10th to16th week reaching about one fifth of the peak value, and remains at the same level until term.[62]

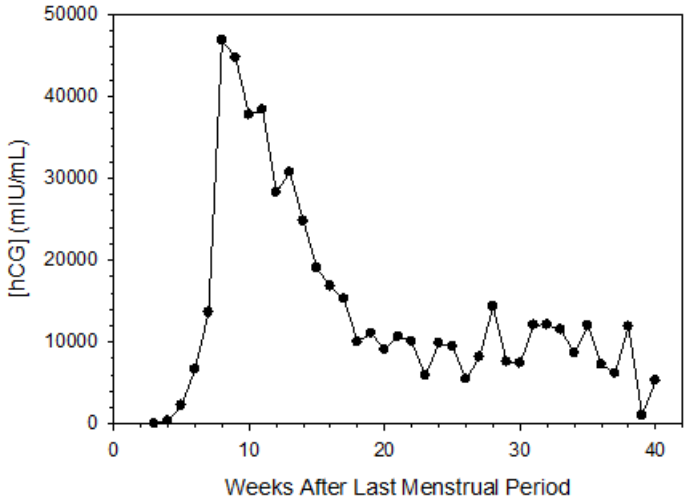

Figure 1.26. The time dependence of hCG concentration.

Therefore, it is very important to monitor the hCG concentration during the whole period of pregnancy.

1.3.3. Methods of hCG measurement

Nowadays, there are mainly two types of commercially used hCG test methods: pregnancy test strip and ELISA. The pregnancy test strip only provides a qualitative result by showing a positive or negative result while ELISA can quantify the hCG amount in a patient's serum or urine sample.

As a well-known point of care (POC) device, the pregnancy test strip has reached a huge success by providing an easy, rather trustable way to test whether a patient is pregnant or not. The lateral-flow assay (LFA) or lateral flow immunochromatographic assay, was employed inside a test strip.[65]

In general, three different kinds of antibodies are involved in the testing process. One kind of antibodies are labeled with gold nanoparticles or dye molecules and immobilized on the conjugate pad zone as shown in Figure 1.27 while the other two kinds of antibodies are immobilized on the control line and test line respectively. The ones that are attached to the test line can bind to the target of interest while the ones attached to the control line are capable of binding to the first kind of antibodies (the labeled ones).

When the sample is added to the sample pad, the analytes, if present, will flow along the strip, be captured by the labeled antibodies and eventually bind to the test line by forming a sandwich structure. If analytes are absent, the control line won't show up. In both cases, the excessive mobilized antibodies will be captured by the antibodies on the control line. Thus, two lines represent for a positive result and one line represents a negative result.

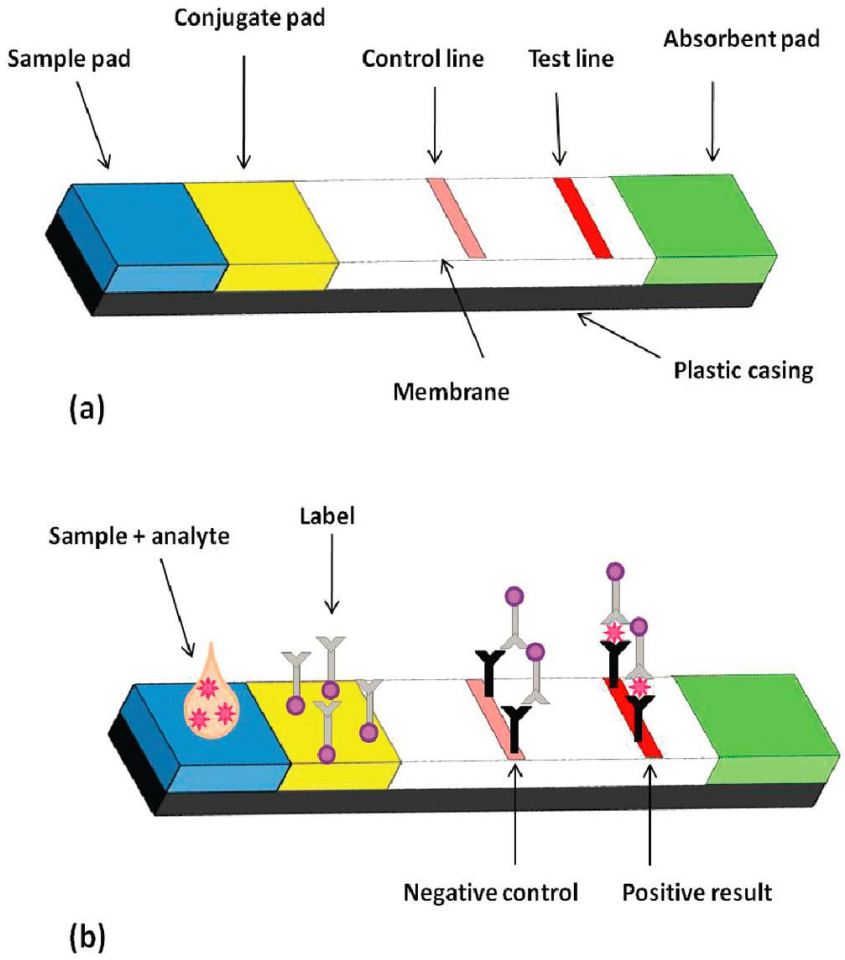

Figure 1.27. Schematic illustration of working principle of pregnancy test strip. (a) The design of a typical lateral-flow immunoassay. (b) After adding samples, the analytes bind to labeled antibodies, flow to the other end of the strip and get captured by the antibodies immobilized on the test line, showing a positive result. If analyte is absent, the labeled antibodies bind to the antibodies immobilized on the control line, showing a negative result.

Note. Reprinted with permission from Gubala, V.; Harris, L. F.; Ricco, A. J.; Tan, M. X.; Williams, D. E. Point of Care Diagnostics: Status and Future. *Anal. Chem.* 2012, *84*, 487–515. Copyright 2012 American Chemical Society.

Today's most conventional quantitative hCG test method is ELISA, which has been considered as the golden standard for pregnancy detection.[66] However, as mentioned before, the ELISA test needs to be done in a biomedical laboratory by well trained technicians, which takes a day or two for running the test and analyzing the data.[67]

1.4. Objectives of this thesis

To address the afore-mentioned shortcomings, such as fussy procedures for labeling antibodies with enzyme, the requirement of expensive equipment as well as well trained technicians, and the lack of portability of ELISA tests, in this work we explored an alternative signal enhancement method for protein detection with electrochemical immunosensors. Instead of labelling the antibodies with fluorophores or redox-active groups, they were labelled with DNA single strands through streptavidin-biotin interaction. The electrochemical signal was generated by the CV responses of surface-bound redox active $[Ru(NH_3)_6]^{3+}$, upon labeling the detecting antibody with DNA strands in a standard sandwich-format immunoassay. Redox-active cations (e.g., $[Ru(NH_3)_6]^{3+}$) are well-known to interact with negatively charged DNA phosphate backbone through electrostatic interaction; upon saturation the integrated charge of surface-bound $[Ru(NH_3)_6]^{3+}$ can be converted to its surface density, which in turn provides an quantitative measure of the antigens detectable in sandwich-format immunoassays. By using electrochemical signal as the readout, this method also bears the merits of good portability and cost effectiveness.

Human chorionic gonadotropin (hCG) detection has been studied as a model analysis. hCG is an important biomarker for a variety of clinical diagnoses such as pregnancy and gynecological cancers. Abnormal hCG concentrations indicate the appearance of some diseases. Therefore, it is very important to monitor the hCG level during the entire pregnancy period.

Chapter 2.

Experimental Section

2.1. Reagents and materials

The human chorionic gonadotropin (hCG) standard samples (100 mIU mL^{-1}), anti-hCGα monoclonal antibody (Mab), and anti-hCGβ Mab, follicle stimulating hormone (FSH), and thyroid stimulating hormone (TSH) standard samples were provided by Biogate Laboratories Ltd. (Burnaby, Canada). Three synthetic oligonucleotides were purchased from Integrated DNA technologies, Inc (Coralville, IA) and their sequences are listed in Table 2.1. Gold substrates (regular glass slides first covered with 5-nm Cr, followed by 100-nm Au) were purchased form Evaporated Metal Films (EMF) Inc. (Ithaca, NY). The biotin labeling kit-NH_2 was purchased from Dojindo Molecular Technologies, Inc. (Rockville, MD). NH_2-PEG_2-biotin, N-Hydroxysuccinimide (NHS), 1-ethyl-3-(3-dimethylaminopropyl) carbodiimide hydrochloride (EDC), N-morpholinoethane sulfonic acid (MES), 6-mercapto-1-hexanol (MCH), 6-mercaptohexanoic acid (MCHA), hexaamminetuthenium (III) chloride (98%), and Tween-20 were purchased form Sigma-Aldrich (Milwaukee WI). MPEG3-NH_2 ($C_7H_{17}NO_3$) was purchased from ChemPep Inc. (Wellington, FL). Deionized water (> 18.3 MΩ cm) was obtained from a Barnstead EasyPure UV/UF compact water system (Dubuque, IA).

Table 2.1. DNA sequences

Name	Sequences
27 mer synthetic oligonucleotide	5'-biotin-GTC CGT GGT AGG GCA GGT TGG GGT GAC-3'
42 mer synthetic oligonucleotide	5'-biotin-ATC TAC GAA TTC ATC AGG GCT AAA GAG TGC AGA GTT ACT TAG-3'
complementary strand for the 42 mer synthetic oligonucleotide	5'- CTA AGT AAC TCT GCA CTC TTT AGC CCT GAT GAA TTC GTA GAT -3'

The buffer solutions had the following compositions: activation buffer: 0.1 M N-morpholinoethane sulfonic acid (MES), pH 5.8; immobilization buffer: 100 mM phosphate buffer, 150 mM NaCl, 5% glycerol, pH 7.4; washing buffer: 100 mM phosphate buffer, 150 mM NaCl, 0.1% gelatin, 0.05% Tween 20, 5% glycerol and 2 mM NaN_3 at pH 7.4.

2.2. Substrate modification and immunosensor preparation

Small pieces of gold slides (0.7 × 2.5 cm) were cleaned by immersion in a Piranha cleaning solution (3:1 mixture of 98% H_2SO_4 and 30% H_2O_2) for 5 min at 90 °C, followed by a rinse with copious amounts of deionized water. *CAUTION: piranha reacts violently with organic solvents, and should be handled with extreme caution.* The gold chips were then dried with N_2. A 15-µL drop of the binary solution of 5 mM MCHA and 10 mM MCH was spread on the freshly cleaned gold substrates and incubated for one hour at 100% humidity. After the immobilization, the gold slides were rinsed with deionized water again, followed by spreading a 15-µL drop of the activation buffer (containing 100 mM EDC and 25 mM NHS) and incubation at room temperature for 3 hours.

The biotin-streptavidin assay was tried first to provide an easier system for optimizing experimental conditions such as streptavidin concentration, and biotin labeled DNA concentration. NH_2-PEG_2-biotin (0.1 M) was attached to the EDC/NHS-treated surface and incubated for one hour. Then streptavidin and biotin-labeled DNA were added and incubated.

For the preparation of the hCG direct assay, the hCG samples in the immobilization buffer were spread on the modified gold slides (15 µL on each slide) and incubated for an hour. Biotin-labeled anti-hCGβ Mab (0.1 µg mL^{-1}) in washing buffer was then added onto each gold chip and incubated for 1 hour. The gold chips were rinsed by washing buffer, followed by adding a drop of 15 µL streptavidin (25 µg mL^{-1}) in washing buffer onto each gold chip and incubating for 1 hour. A 15 µL drop of 3 µM biotin-labeled DNA strands in TE buffer (10 mM Tris, 1 mM EDTA, pH 8) was spread on each gold chip and incubated for one hour after washing away the unreacted streptavidin.

For the preparation the hCG sandwich assay, a 15-μL drop of the probe antibody, anti-hCGα Mab (50 μg mL^{-1}) in the immobilization buffer was spread on each gold chip and kept overnight at 100% humidity. Unbound anti-hCGα Mab was later washed away by using immobilization buffer. The unreacted carboxyl groups on the surface were blocked by reaction with 0.1 M MPEG3-NH_2 (15 μL on each gold chip) for an hour. The hCG samples in the immobilization buffer were then spread on the modified gold slides (15 μL on each slide) and incubated for an hour. Biotin-labeled anti-hCGβ Mab (0.1 μg mL^{-1}) in washing buffer was then added onto each gold chip and kept for 1 hour. The gold chips were rinsed by washing buffer, followed by adding a drop of 15 μL streptavidin (25 μg mL^{-1}) in washing buffer onto each gold chip and incubating for 1 hour. A 15-μL drop of 3 μM biotin-labeled DNA strands in TE buffer (10 mM Tris, 1 mM EDTA, pH 8) was spread on each gold chip and incubated for 1 hour after washing away the unreacted streptavidin.

For the double-stranded DNA labeling, the biotin-labelled DNA strand was hybridized with its complementary strand in hybridization buffer (10 mM Tris, 150 mM NaCl, 3 mM $MgCl_2$) by incubating at 80 °C for 5 minutes, followed by slowly cooling down to room temperature over a period of 60 minutes to form biotin-labelled double-stranded DNA.

2.3. Electrochemical measurements

Cyclic voltammetry (CV) measurements were performed with a CHI 660D electrochemical workstation (CH Instruments Inc.) using a three-electrode single chamber cell made of Plexiglas V-series acrylic resin. The modified working electrode was pressed against an O-ring seal (with an exposed area of 0.126 cm^2) at the side of the cell. A platinum wire and an Ag | AgCl | 3 M NaCl electrode were used as the counter electrode and reference electrode, respectively.

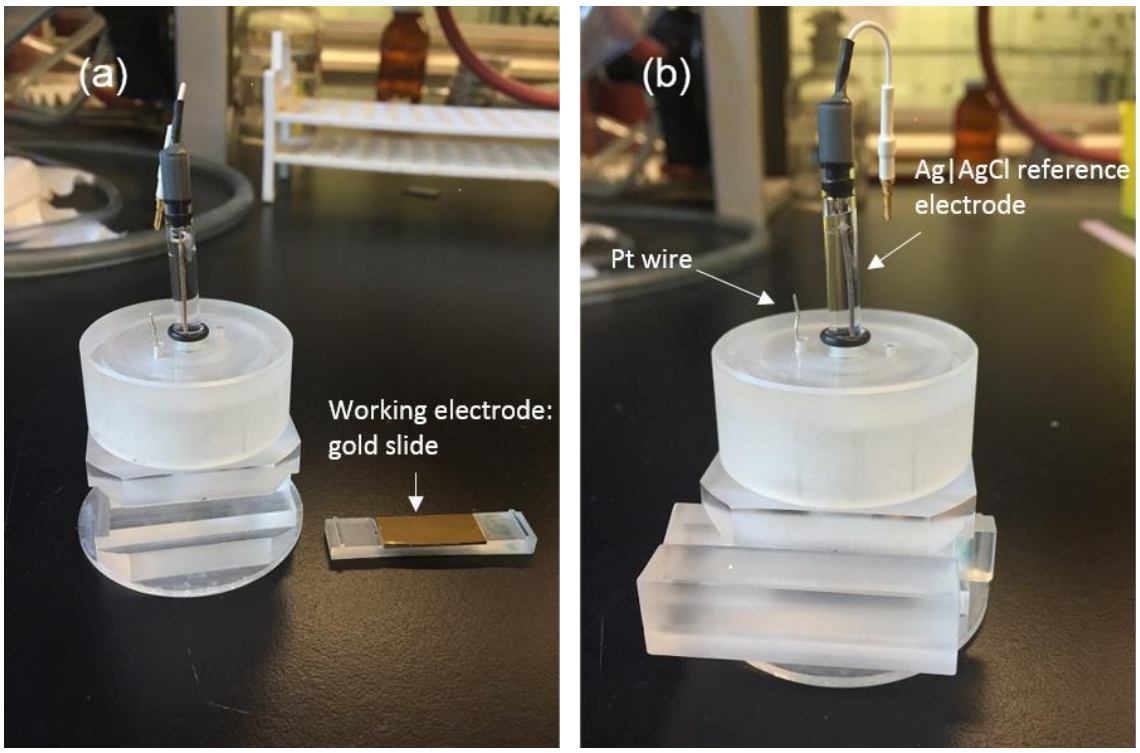

Figure 2.1. Three-electrode single-chamber cell used for electrochemical measurements. Platinum counter electrode and Ag| AgCl | 3 M NaCl reference electrode are placed into the cell through the holes on top of the chamber cell lid. (a) The gold slide is placed separately from the cell. (b) The gold slide is assembled to the chamber cell body part.

All electrochemical measurements were performed with 5.0 μM $[Ru(NH_3)_6]Cl_3$ in 10 mM Tris-HCl buffer at pH 7.4 under ambient conditions (21-23 °C). The supporting electrolyte was deoxygenated by bubbling Argon for at least 15 min prior to the measurement.

Chapter 3.

Results and Discussion

3.1. Surface activation and biotin-streptavidin assay

For the purpose of optimizing the reaction time for each step as well as applying a reasonable amount of reagents, the NH_2-PEG2-biotin system was tried out first. In order to simplify the experimental system, NH_2-PEG2-biotin was used as replacement for the capture antibody-antigen-detection antibody as shown in the figure below.

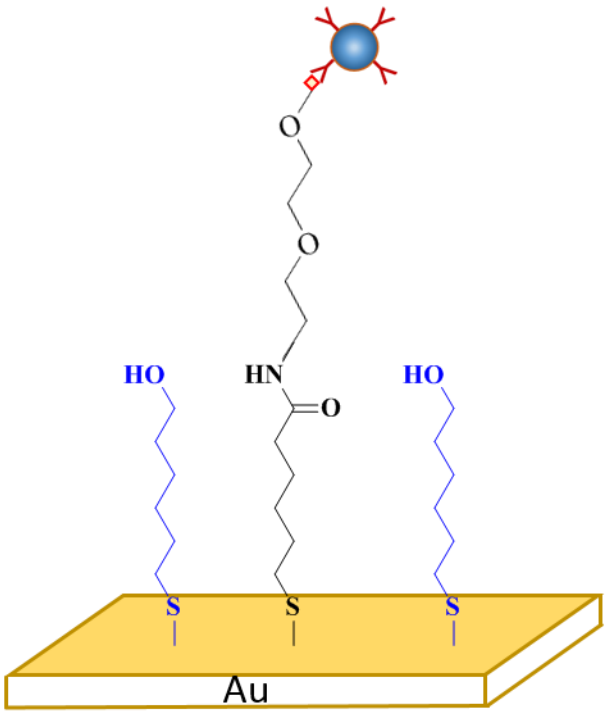

Figure 3.1. Pictorial illustration of the NH_2-PEG2-biotin system. The amine group was linked to the EDC/NHS-treated surface through amide coupling. The biotin molecule is represented by the red rectangle.

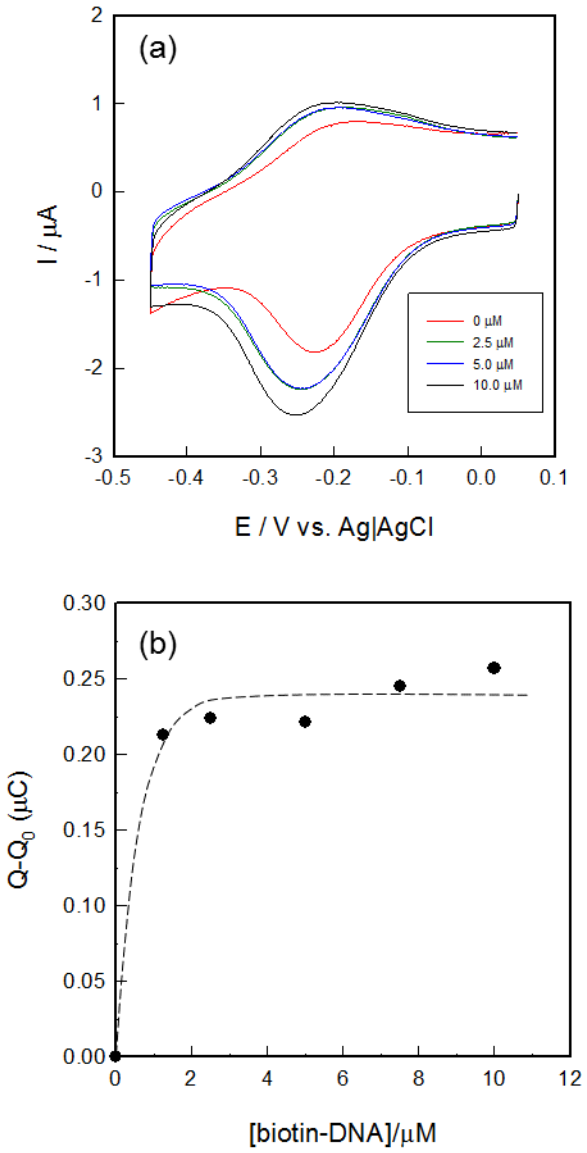

Figure 3.2. Optimization of biotin-labeled DNA concentration. (a) Cyclic voltammograms of 5.0 µM [Ru(NH3)6]3+ on the NH_2-PEG2-biotin system in 10 mM Tris buffer at pH 7.4 after incubation with different concentrations of biotin-DNA: 0, 2.5, 5.0, 10.0 µM. (b) Signal increase as a function of biotin-DNA concentrations. Saturation is observed at 3.0 µM. The dashed trend line was added to guide the eyes.

After the attachment of biotin molecules to the surface, streptavidin was added. The last step for electrode modification is the addition of biotin-labeled DNA strands. The modified electrodes were tested by cyclic voltammetry in 5 µM $[Ru(NH_3)_6]^{3+}$. As shown in Figure 3.2(a), clear-cut CV signals were produced at the modified electrodes. Because

the potential changes linearly with the time, by integrating the cathodic peak of the cyclic voltammogram, the charges (Q) were calculated. The background signal Q_0 was calculated when no biotin-DNA was added to the system.

The signal increase ($Q-Q_0$) was plotted against the concentration of biotin-DNA. From figure 3.2(b) it can be observed that with increasing the biotin labeled DNA concentration, the signal increase initially and then remain constant after the concentration reaches 3.0 μM. Therefore, the concentration for biotin labeled DNA was chosen as 3.0 μM.

3.2. hCG direct immunoassay

As shown in the figure below, a direct immunoassay was designed to be constructed on gold electrode for the detection of protein. hCG has been used as a model system.

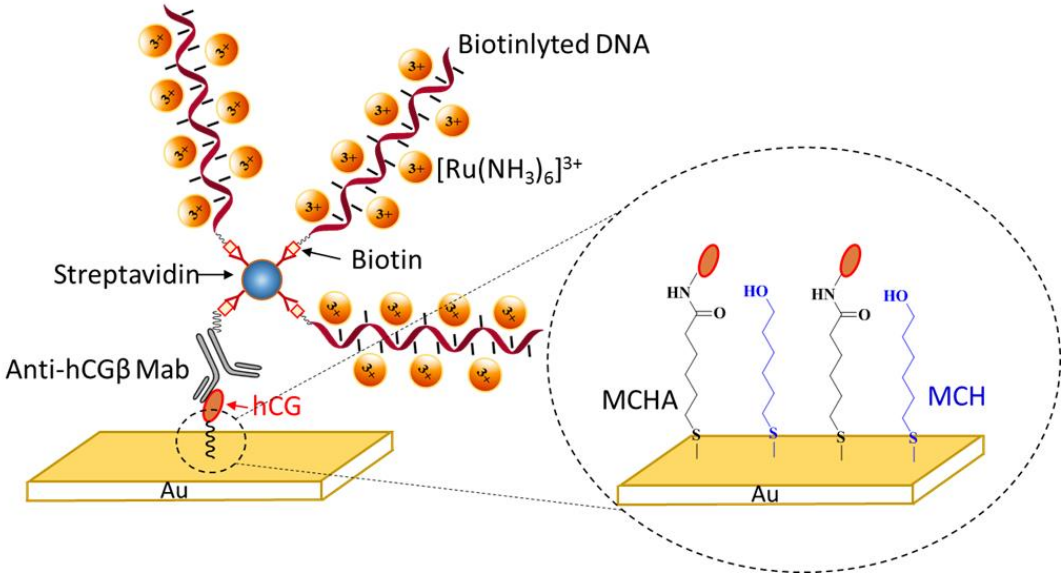

Figure 3.3. Design of the DNA-enhanced electrochemical direct immunoassay for protein detection. Inset: hCG were attached to the gold surface by amide coupling with carboxyl groups on a mixed MCHA/MCH monolayer.

The direct immunoassay experiments were carried out as a preliminary study of the performance of hCG and its antibodies.

Here in Figure 3.4 the cyclic voltammograms of 5.0 µM $[Ru(NH_3)_6]^{3+}$ on modified gold electrodes are shown which had been incubated with different hCG concentrations. The cathodic peak appeared at -0.25 V vs. Ag|AgCl in the absence of hCG and exhibited a gradual shift towards the negative direction when hCG was present, which indicates that binding between DNA strands and $[Ru(NH_3)_6]^{3+}$ happened. The cathodic peak area of $[Ru(NH_3)_6]^{3+}$ increased with growing hCG sample concentrations, confirming the accumulation of redox cations on the DNA strands.

The background signal is not negligible as shown in the CV voltammograms, which is believed to be caused by the non-specific binding between the redox cation $[Ru(NH_3)_6]^{3+}$ and the capture antibodies. Another possible reason is the non-specific binding of the detection antibodies to the surface, which also resulted in the attachment of DNA strands to the surface through biotin-streptavidin interaction.

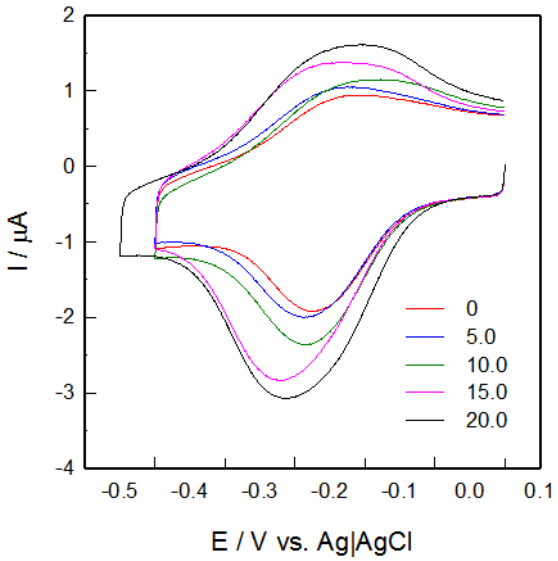

Figure 3.4. Cyclic voltammograms of 5.0 µM $[Ru(NH_3)_6]^{3+}$ on the direct immunoassay modified gold electrodes in 10 mM Tris buffer at pH 7.4 after incubation with different concentrations of hCG: 0, 5.0, 10.0, 15.0, 20.0 mIU/mL.

As shown above, the cathodic peak area increases with increasing concentration of hCG. In order to study the detection limit and detection range of this direct immunoassay, the dependence of relative signal increase (S) obtained by integration of the reduction peak of $[Ru(NH_3)_6]^{3+}$ in the cyclic voltammograms before (Q_0) and after (Q)

incubation with hCG, $S=(Q-Q_0)/Q_0$ on hCG concentration has been plotted and is shown as below in Figure 3.5.

The cathodic peak and anodic peak are not symmetric as shown in Figure 3.4. The binding constant of $[Ru(NH_3)_6]^{2+}$ to DNA strands is smaller than $[Ru(NH_3)_6]^{3+}$, resulting a smaller peak area. In order to ensure the accuracy, anodic peak is not used for the quantification.

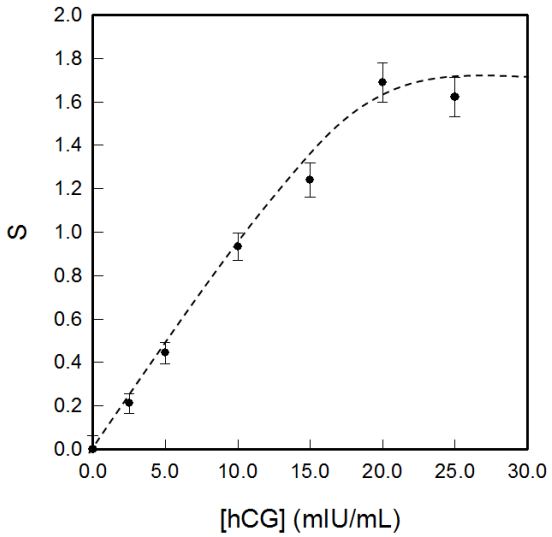

Figure 3.5. Relative signal increase as function of hCG concentration The dash line was added to guide the eyes.

The plot shows the relative signal increase with rising concentration of hCG and gets approach to saturation when the concentration reached 25.0 mIU/mL of hCG.

Selectivity tests were also carried out. The two hormones, TSH and FSH, were chosen as a comparison to hCG. All three hormones were tested by the same experimental procedures. The concentration of each hormone was chosen to be higher than the regular hormone level in human fluids. The results show that the effect of TSH barely influenced the detection of hCG. However, due to the direct immobilization of a high FSH concentration on the surface, $[Ru(NH_3)_6]^{3+}$ could be adsorbed to the FSH hormone and contribute a rather high background. Therefore, the sandwich-format immunoassay was further studied to avoid this shortcoming.

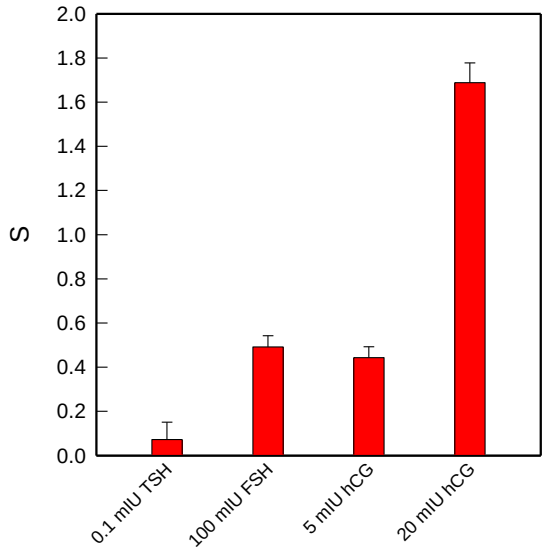

Figure 3.6. Comparison of relative signal change caused by hCG and other hormones (TSH, FSH) in the direct immunoassay.

To further confirm the advantage of using DNA-redox cation interactions for signal enhancement, direct immunoassay experiments were performed with DNA strands of different length. The double-stranded DNAs were hybridized in solution before usage.

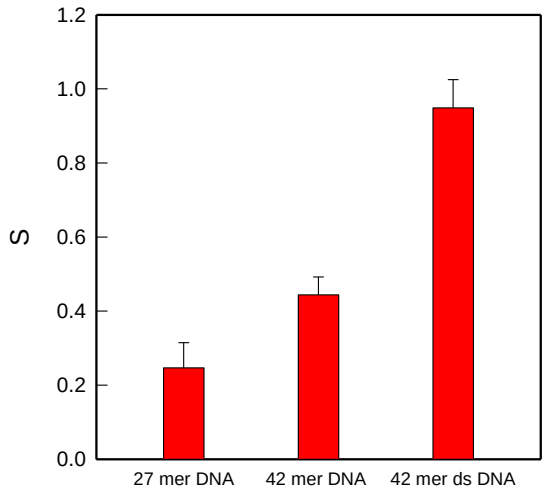

Figure 3.7. Comparison of signal intensities obtained with DNAs of different lengths in the direct immunoassay. From left to right: 27 mer single-stranded DNAs, 42 mer single-stranded DNAs, and 42 base pairs double-stranded DNAs.

There is a clear signal difference between the 27-mer single-stranded DNA and the 42-mer single-stranded DNA. The 42-mer double-stranded DNA also showed a stronger signal than the 42 mer single-stranded DNA. These results validate the proposed signal enhancement strategy by employing DNA-$[Ru(NH_3)_6]^{3+}$ interactions.

However, because the direct assay cannot be used to test the real samples such as serum or other human fluids, the sandwich immunoassay was further studied.

3.3. hCG sandwich-format immunoassay

As shown in Figure 3.8, a sandwich-format immunoassay was designed and constructed on a gold electrode for the detection of protein and hCG detection was used as a model system.

3.3.1. Sandwich-format immunoassay design and its electrochemical performance

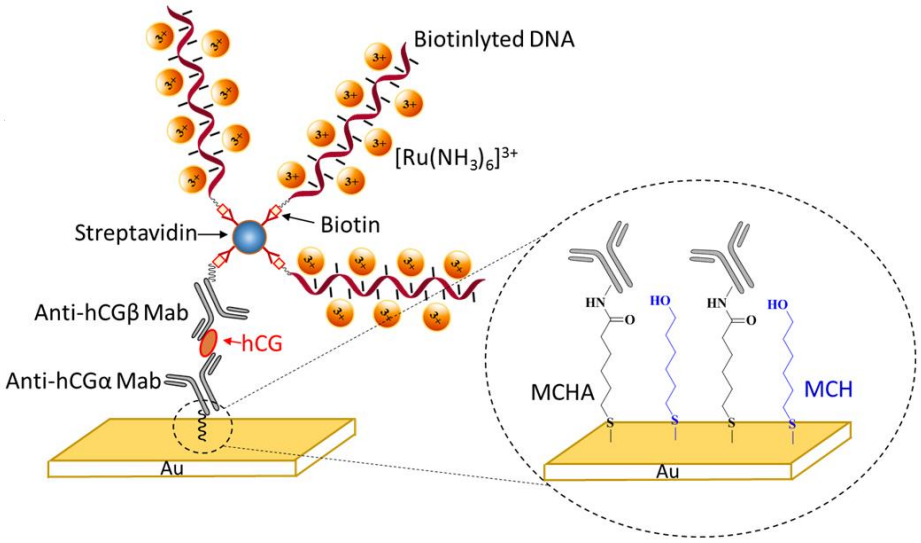

Figure 3.8. Design of the sandwich-format DNA-enhanced electrochemical immunoassay for protein detection using hCG as a trail analyte. Inset: anti-hCGα Mab were attached to the gold surface by amide coupling with carboxy groups on a mixed MCHA/MCH monolayer (right inset).

Two different monoclonal antibodies were employed in the detection: the capture antibody anti-hCGα Mab and the detecting antibody anti-hCGβ Mab. As previously mentioned, hCG is a heterodimer consisting of an hCGα subunit and an hCGβ subunit. Due to the fact that there are several epitope binding sites on an hCG dimer, the anti-hCGα Mab can recognize and bind to not only the hCGα subunit but also the hCG dimer; anti-hCGβ Mab can bind to the hCGβ subunit, the hCG β-core fragment, and the hCG dimer.[68] Therefore, the capture antibody recognizes all of these hormones and subunits and only intact hCG can be further captured by the detection antibody.

These monoclonal antibodies were generated from hybridoma cells. To be more specific, the spleen cells of the host animal (mouse) were taken out and fused with myeloma cells after immunizing the mouse against human hCGα and hCGβ molecules by intraperitoneal injection over a period of weeks after which the fused hybridoma cells were separated and individually cultured. When desired antibodies were present as demonstrated by screening, the specific hybridoma cell could be cultured and monoclonal antibodies could be harvested from it.

A mixed self-assembled monolayer (SAM) of 6-mercaptohexanoic acid (MCHA) and 6-mercapto-1-hexanol (MCH) on gold served as both the provider of carboxyl groups and as spacers to reduce the surface density of the active sites. To promote the immobilization of probe antibodies, the surface was treated with EDC and NHS to activate the carboxyl groups. It is also important to note that to reduce the potential nonspecific adsorption, the unreacted carboxyl groups were blocked by reaction with MPEG3-NH_2 ($C_7H_{17}NO_3$). Unlike a standard ELISA assay, the detection antibody was labeled with a biotin group. As depicted in Figure 3.8, multiple DNA strands were attached to the sandwich structure via the binding of streptavidin to the surface. The fact that each streptavidin has four biotin-binding sites, we expected that up to three biotinlyted DNA strands would be attached to a single detection antibody. After the whole assay was constructed, the electrochemical response of the system in 5.0 μM $[Ru(NH_3)_6]^{3+}$ was measured by cyclic voltammetry (CV).

A schematic illustration of the sandwich-format assay preparation procedure is shown in Figure 3.9.

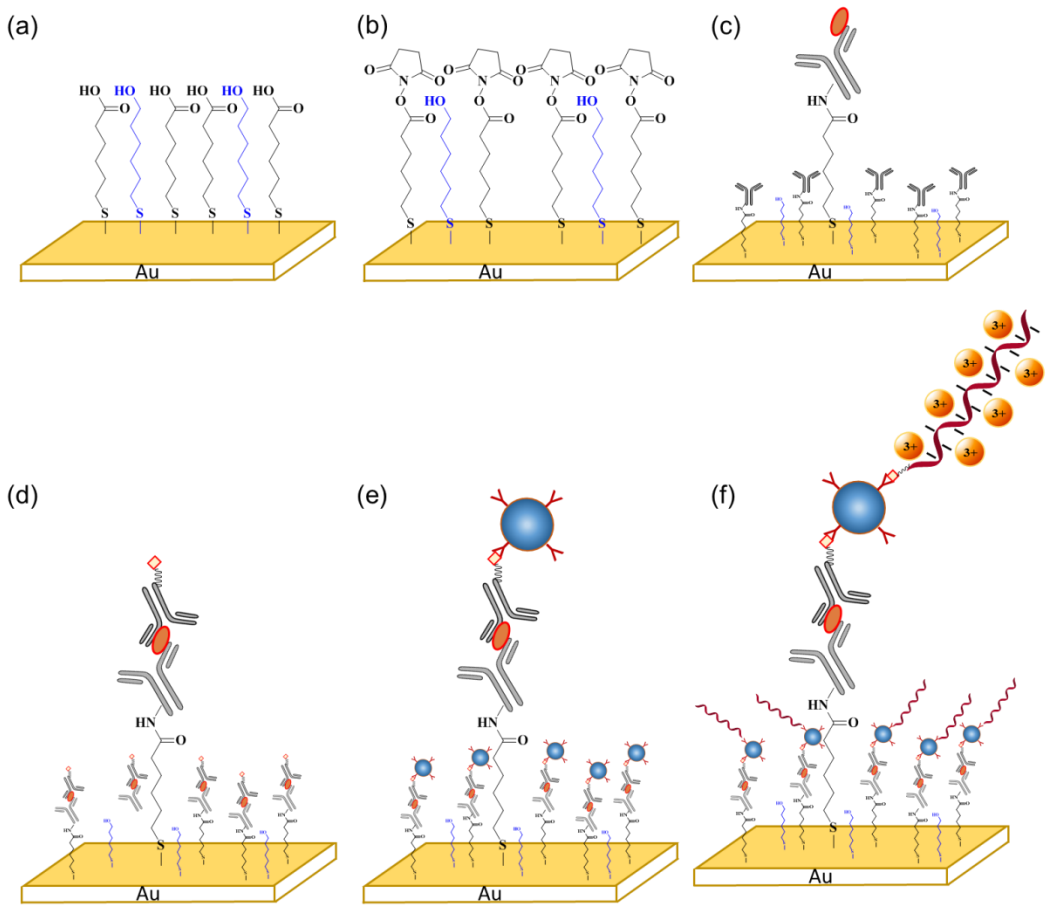

Figure 3.9. **Scheme of the sandwich-format assay preoaration. (a) Immobilize a 2:1 mixture of MCHA and MCH on freshly cleaned gold slides. (b) Activate carboxyl groups by treatment with EDC and NHS. (c) Attach the anti-hCGα Mabs to the gold surface via amide-coupling (d) The surface bound anti-hCGα Mabs capture hCG samples, which later are detected by biotin-labelled anti-hCGβ Mabs. (e) Bind streptavidin to the gold surface by biotin-streptavidin interaction. (f) Bind the biotin-labelled DNA to the free binding sites of streptavidin. The modified gold slides were tested in 5.0 μM $[Ru(NH_3)_6]^{3+}$ by cyclic voltammetry.**

The CV responses of the sensor's electrodes which had been incubated with different concentrations of hCG standard samples in the presence of 5.0 μM of $[Ru(NH_3)_6]^{3+}$ are shown in Figure 3.10.

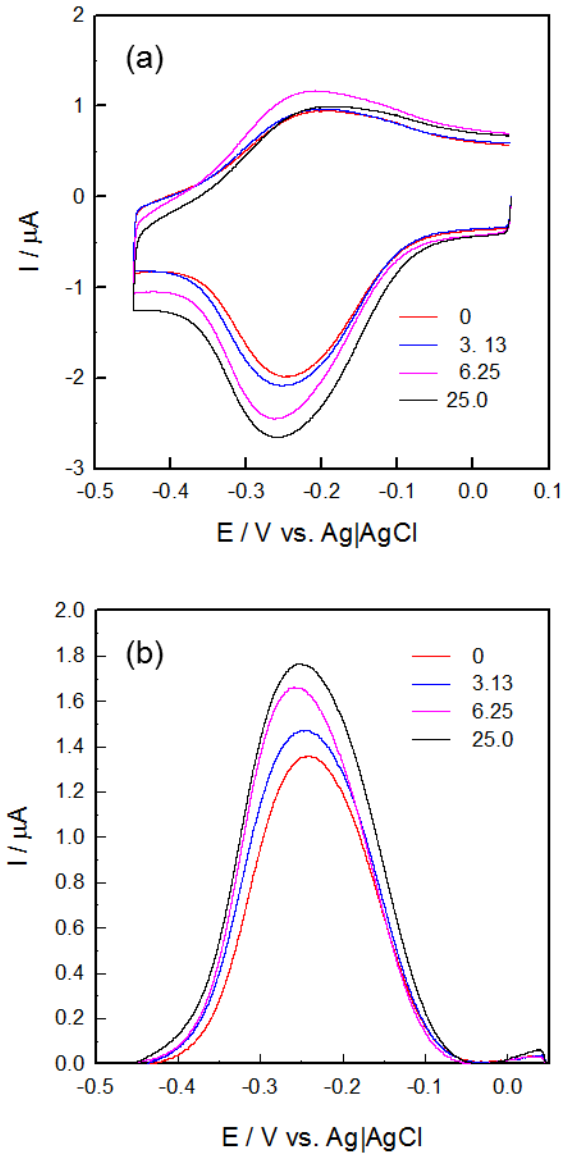

Figure 3.10. (a) Cyclic voltammograms of 5.0 µM $[Ru(NH_3)_6]^{3+}$ on the sandwich-format immunoassay modified gold electrodes in 10 mM Tris buffer at pH 7.4 upon incubation with different concentrations of hCG. (b) Normalized cathodic peaks at four representative concentrations of hCG: 0, 3.13, 6.25, 25.0 mIU/mL.

As shown in the above figure (b) the cathodic peak area (i.e., reduction of $[Ru(NH_3)_6]^{3+}$ to $[Ru(NH_3)_6]^{2+}$) increased monotonically with increasing hCG concentration. The cathodic peak appeared at -0.25 V vs. Ag|AgCl in the absence of hCG and exhibited a gradual shift towards the negative direction. Such a formal potential shift shows the

rather strong electrostatic interaction between DNA strands and $[Ru(NH_3)_6]^{3+}$, particularly the different binding affinities of the oxidised ($[Ru(NH_3)_6]^{3+}$) and the reduced forms ($[Ru(NH_3)_6]^{2+}$).[26,69]

$$\Delta E^{\circ\prime} = -\frac{RT}{nF}\ln(K_{ox}/K_{red}) \quad (3\text{-}1)$$

The gradual increase in cathodic peak currents further suggested the accumulation of redox cations in the DNA layer. Accompanied by higher concentrations of hCG, the formal potential shifted slightly to more negative values, showing the differences in binding strength between $[Ru(NH_3)_6]^{3+}$ and DNA with increased surface densities. The non-zero background signal and the cathodic peak with no analyte added, indicate the binding of $[Ru(NH_3)_6]^{3+}$ to the capture antibodies or direct interaction between the probe and detection antibodies. Another possibility is the electrostatic interaction between capture and detection antibodies. A third possibility is electrostatic interaction between $[Ru(NH_3)_6]^{3+}$ and unreacted carboxyl groups of the mixed MHA/MCH monolayer.

To quantitatively characterize the detection limit and the detection range, the relative increase in the integrated charge of the reduction peak was determined. In particular, the dependence of the relative signal increase (S) obtained by integration of the reduction peak of $[Ru(NH_3)_6]^{3+}$ in the cyclic voltammograms before (Q_0) and after (Q) incubation with hCG, $S=(Q-Q_0)/Q_0$ is shown as a function of hCG concentration. The concentration of hCG was plotted and is shown in figure 3.11. A clear increase of the sensor signal accompanied the hCG concentration increase. The sensor signal reached saturation when the concentration of hCG increased to 25 mIU/mL, in which case we could determine the saturated sensor signal, $S_{sat} = (Q_{max} – Q_0)/Q_0$. At low concentrations (0 to 12.5 mIU/mL), the relative signal increase may be considered proportional to the hCG concentration within the experimental uncertainties. The detection limit of this sandwich-format immunosensor was estimated to be 1.25 mIU/mL of hCG, which is three times the standard deviation of the signal. It is noteworthy that this detection limit is comparable to that of the conventional ELISA test.[70]

For a better understanding of the antigen-antibody interaction on the surface, the adsorption isotherm of hCG binding to anti-hCGα monoclonal antibodies was further studied. Assuming the binding process meets the requirements of the Langmuir isotherm, the dissociation constant (K_d) can be calculated from:

$$\mathrm{Mab|gold} + \mathrm{hCG} \rightleftharpoons \mathrm{Mab \bullet hCG|gold} \tag{3-2}$$

$$K_d = [\mathrm{Mab}][\mathrm{hCG}]/[\mathrm{Mab \bullet hCG}] \tag{3-3}$$

where [Mab] and [Mab•hCG] are the surface concentrations of unbound and bounded anti-hCGα Mabs upon reaching binding equilibrium. If we define θ, the fractional occupancy, as the ratio between bound Mab to the total surface concentration of Mab, [Mab•hCG]/([Mab]+[Mab•hCG]), the above equation can be rearranged to

$$\theta = \frac{[\mathrm{hCG}]}{K_d + [\mathrm{hCG}]} \tag{3-4}$$

Because the amount of [Mab•hCG] adsorbed onto the surface is proportional to the electrochemical signal S defined above, θ can be obtained from:

$$\theta = \frac{S}{S_{sat}} \tag{3-5}$$

Then we have,

$$\frac{S}{S_{sat}} = \frac{[hCG]}{K_d + [hCG]} \tag{3-6}$$

However, in a sandwich assay, both capture antibodies and detection antibodies affect the binding behavior of the antigen; herein we only consider the first step binding by assuming similar affinities of the two antibodies to hCG. Therefore, we went ahead to apply the following equation to estimate the K_d value.[71–73]

$$\frac{[hCG]}{S} = \frac{[hCG]}{S_{sat}} + \frac{K_d}{S_{sat}} \tag{3-7}$$

The Figure below shows that [hCG]/S is indeed proportional to [hCG], which indicates that the binding process does follow the Langmuir isotherm. From the linear fit, K_d was calculated to be (2.2±0.2) $\times 10^{-11}$ M, which is in agreement with the hCG dissociation constant determined by Englebienne et al. in 1998.[74]

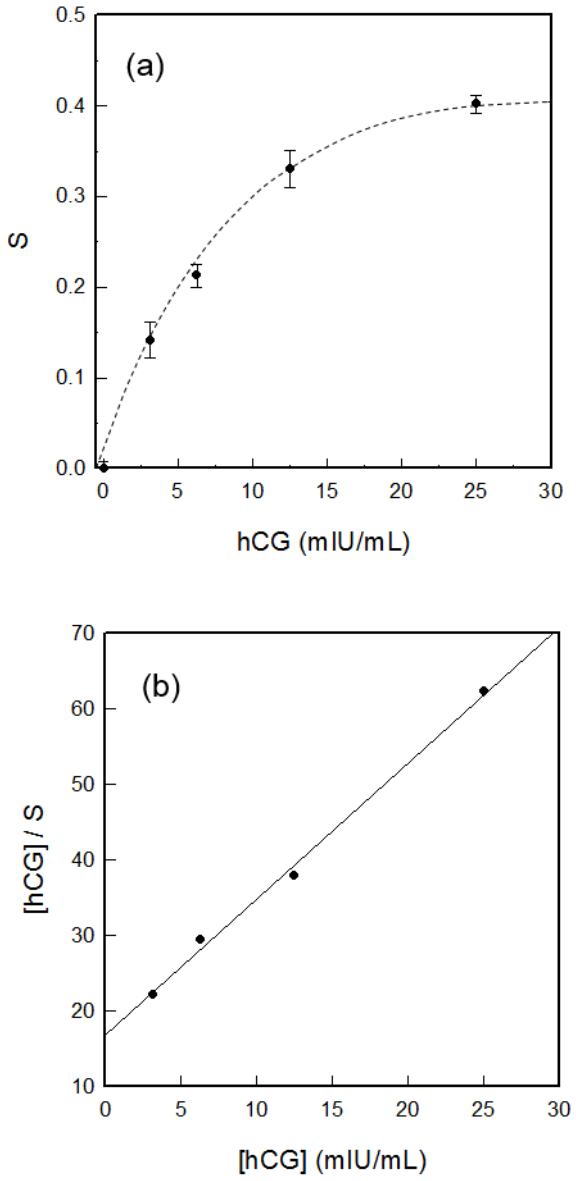

Figure 3.11. (a) The relative signal increase (S) as a function of concentration of hCG. (b) Linearized adsorption isotherm of hCG binding to anti-hCGα Mabs on the gold electrode based on the Langmuir model. The solid line is the best fit to the experimental data from which the dissociation constant K_d was determined.

The K_d value in this study was found to be slightly smaller probably due to the low surface density of antibody. Besides the determination of the binding affinity, it was also useful to determine the DNA surface density, Γ_{DNA}, at least when the highest concentration of hCG was tested. Based on the integrated charge of surface-bound $[Ru(NH_3)_6]^{3+}$,the DNA surface density was calculated to be $(6.1\pm1.0)\times10^{11}$ molecules/cm^2 by using equations (1-15) and (1-16).

The low surface density of DNA confirmed that the amount of immobilized anti-hCGα Mabs was much less than the theoretical amount (<1/30).[75] In fact this might have helped to minimize the possibility of steric hindrance. As a result, the efficiency of steric hindrance among the rather large antibodies is low and the binding between anti-hCGα antibodies and hCG appears to be as strong as that in solution.

Having shown the sensitivity enhancement of the hCG immunoassay by DNA-redox cation interaction, the next task is to confirm that other hormones would not hinder its performance. Herein, the following results of selectivity tests have been shown. Two hormones, follicle stimulating hormone (FSH) and thyroid stimulating hormone (TSH) were chosen as comparison to hCG for the reason that the alpha subunit of hCG is identical to that of FSH and TSH while the beta subunit is unique to hCG. The normal range of TSH in human bodies is 0.4-4.0 μIU/mL while normal FSH levels differ depending on a person's age and gender: for male subjects, the normal range is 0 to 12.4 mIU/mL and for female subjects who are still menstruating, the normal range is 4.7-21.5 mIU/mL. The concentrations of TSH and FSH were chosen to be at least five times higher than the normal value in the selectivity tests.

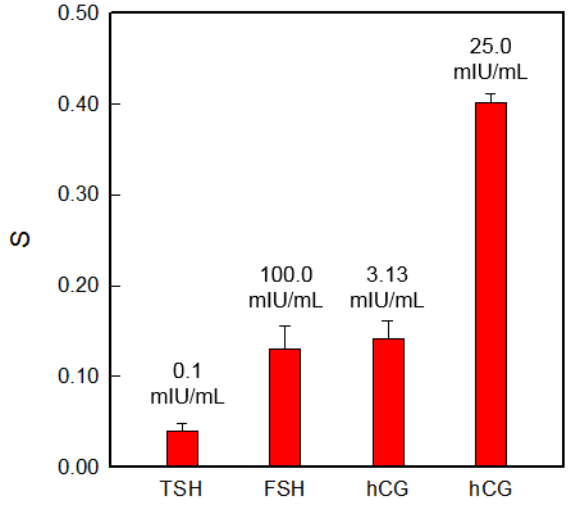

Figure 3.12. Comparison of the sensor signal of hCG and two other hormones (TSH, FSH) with the sandwich-format immunoassay.

Figure 3.12 shows that 0.1 mIU/mL TSH barely influenced the hCG detecting system while 100 mIU/mL FSH slightly affected the performance of this sandwich-format immunosensor. However, this influence would be insignificant if such a high concentration of FSH were applied in real-world tests. Considering that FSH is an acidic protein in the human body with a pI value of 3.3 to 5.8; under the experimental conditions, FSH would be negatively charged and bound to the redox cation $[Ru(NH_3)_6]^{3+}$, resulting in a rather higher background compared to TSH.[68]

To further verify the idea of using DNA-redox cation interactions for signal enhancement, a sandwich-format immunoassay was constructed with DNA strands of different lengths. We found that the signal from 27-mer single-stranded DNAs was not much different from that obtained from 42-mer single-stranded DNAs. In contrast, the 42-mer double-stranded DNAs produced a higher signal, almost twice as strong as the signal from 42-mer single-stranded DNAs.

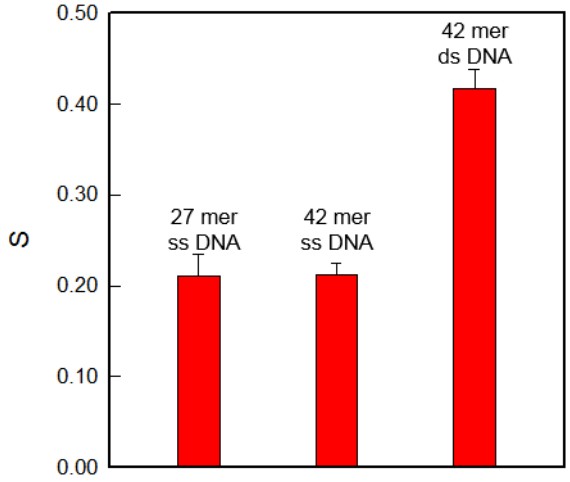

Figure 3.13. Signal comparison for the sandwich-format immunoassay with DNAs of different lengths. From left to right: 27 mer single-stranded DNAs, 42 mer single-stranded DNAs, and 42 base pairs double-stranded DNAs.

The 42-mer single-stranded DNAs showed only a slightly higher signal than 27 mer single-stranded DNAs, which is rather surprising. This could be the result of steric hindrance by the longer DNA chain. It may be easier for the 27-mer DNA strands to form a DNA layer without interfering with other strands, and the electrostatic repulsions may be more pronounced for the 42-mer ones. Considering all the possibilities, it is reasonable that 42-mer DNA strands do not bind more $[Ru(NH_3)_6]^{3+}$ cations (although in principle it should produce a 1.5 times higher signal than the 27-mer strand). As for the double-stranded DNAs, the results indicate a nicely enhanced signal compared to the single-stranded DNAs. This could be due to the higher negative charge density of the double helixes whose phosphate backbones are more oriented towards the solution. Therefore, the electrostatic interaction between them and $[Ru(NH_3)_6]^{3+}$ cations is more predominant than in the single-stranded DNAs.

In order to have a better understanding of the fact that 42-mer single-stranded DNA only showed a lightly increase in the signal, additional data points should be collected from single-stranded DNAs with different lengths such as 7 mer, 17 mer, and 37 mer. In this way, the influence from the steric hindrance for the incorporation of labeling DNA strands to sandwich assay can be further clarified.

Nevertheless, using double-stranded DNA for signal enhancement may lead to additional difficulties for practical applications. As a hybridization step is needed for the formation of double stranded DNA, longer assay times as well as more stringent experimental conditions are required. Due to the fact that the use of 27-mer single stranded DNA meets the needs of simplicity while still showing satisfactory results, all the following experiments were carried out with 27-mer single-stranded DNA. The ideal DNA strand length for maximum signal deserves further studies with strands of different lengths and sequences.

3.3.2. Real sample testing and validation

All afore-mentioned tests have been carried out in standard buffer solutions despite the fact that real-world samples are usually containing impurities and many interfering species. In particular, a patient's urine samples are typically tested for hCG quantification detection. In order to prove the applicability to real-world samples, urine samples from a pregnant woman's 24th to 57th day of gestation have been tested by the sandwich-format immunoassay. Subsequent comparison with ELISA results was also performed. The signal obtained by the electrochemical method showed a clearly increasing trend in the early pregnancy days (from the 24th to the 40th day). Then the hCG level remained relatively stable between the 40th and 50th day after which, the hCG amount started to rise again. During the same time period, the ELISA results also showed the same trend except for revealing slightly higher hCG amounts. It is expected that the hCG level increases exponentially after conception and implantation until week 8,[63] which also has been confirmed previously in our DVD-based bioassay studies.[66]

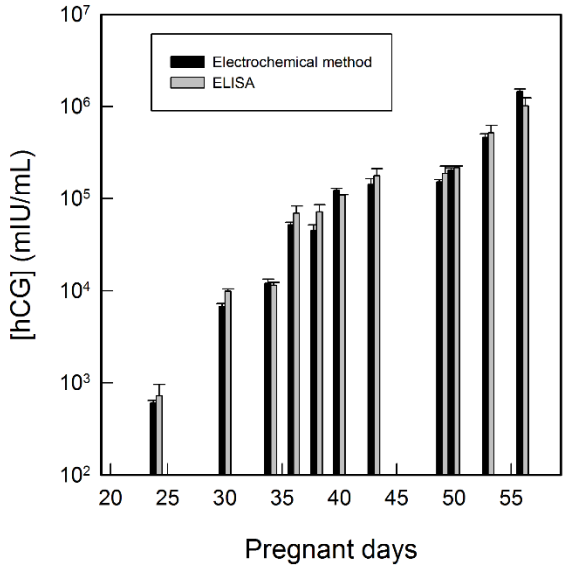

Figure 3.14. Quantitation of urine hCG level of a pregnant woman after various pregnancy days as measured by two different methods. (electrochemical immunoassay and ELISA)

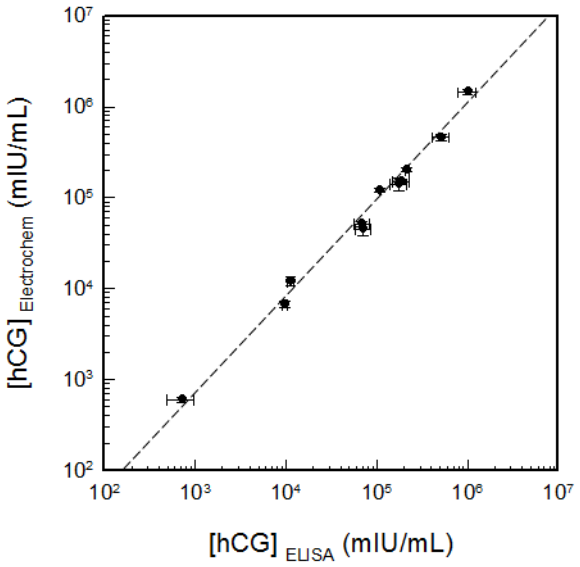

Figure 3.15. Correlation between the hCG concentrations determined by the electrochemical method and by ELISA from the data shown above. The dash line indicates the best fit with R^2=0.99.

For a better understanding of the correlation between the results obtained by the electrochemical method and by ELISA, we have plotted the correlation between the concentrations determined by the two methods for the same set of samples (Figure 3.15). The slope of the best fitting line was calculated to be 0.90±0.03, which indicates that the hCG amounts determined by the electrochemical method are very close to those determined by ELISA. The slightly lower values (indicated by non-unity slope) are probably due to the time difference of running the two sets of tests. The de-freezing processes may speed up the degradation of hCG in the urine sample, resulting in the observed minute difference between the two methods. The constantly lower results obtained by the electrochemical method confirm this assumption. The determination coefficient, R^2, was calculated to be 0.99, which further confirms that the electrochemical method is comparable to the widely applied ELISA method for quantitative analyses.

As mentioned before, the hCG detection is merely a model system to prove that the DNA-redox cation interaction-based signal enhancement strategy works well. Other analytes could be tested by using the similarly designed electrochemical immunoassay with the same signal enhancement approach. It should be noted that there are still other limitations of the DNA-enhanced electrochemical immunoassay method, such as the high background signal and rather narrow detection range.

We have shown that the proposed electrochemical immunoassay still has some limitations, such as high background signal and a rather narrow detection range. Further improvements are desirable to overcome those shortcomings and enhance the immunoassay’s performance.

Chapter 4.

Conclusions and Future work

4.1. Conclusions

Herein, a novel electrochemical method for protein detection has been developed based on a DNA-redox cation interaction enhancement strategy. Instead of labelling the antibodies with fluorophores or redox active groups, the proteins were labeled with DNA single strands; we simply relied on the electrostatic interaction between redox cations ($[Ru(NH_3)_6]^{3+}$) and negatively charged DNA backbone. Human chorionic gonadotropin (hCG) detection has been studied as a model system. A response range up to 25 mIU/mL and a detection limit of 1.25 mIU/mL have been determined that are comparable to the results of the enzyme-linked immunosorbent assay (ELISA) for hCG quantitation. It also shows a good selectivity towards hCG relative to other hormones such as thyroid stimulating hormone (TSH) and follicle stimulating hormone (FSH). Our approach bears the merits of cost effectiveness and simplicity of instrumentation in comparison with conventional optical detection methods.

4.2. Future work

In order to mitigate the high background problem, further optimization of experimental conditions should be attempted, such as controlling the reaction temperature and pH value or using other hCG antibodies that have less acidic pI values to weaken the interaction between $[Ru(NH_3)_6]^{3+}$ cations and antibodies.

In the selectivity tests, TSH and FSH showed some influence on the detection of hCG in both the direct and sandwich assays. In order to minimize the influence from TSH and FSH, anti-hCG β Mabs can be immobilized onto the gold surface instead of

anti-hCGα Mabs. TSH and FSH should not bind to the anti-hCG β Mabs because they have different β subunits from hCG. In this way, the interfering signal from TSH and FSH can be further reduced.

Also, considering that the detection range for hCG never exceeded 25 mIU/mL, one of the most likely reasons is the low percentage of successfully immobilized anti-hCG α Mabs. The binding sites of anti-hCG α Mabs were hindering each other or blocked by the gold electrode. Therefore, instead of modifying the gold electrode with –COOH groups and linking them to the $–NH_2$ groups on antibodies, I can try to modify the gold surface with $–NH_2$ groups and link them with the carboxyl groups on antibodies to achieve a better orientation of antibodies and increases the detection range.

However, modified gold surface with $–NH_2$ groups may also result in the electrostatic interaction between the positively charged $–NH_3^+$ with negatively charged DNA phosphate backbone under the experimental conditions. A good blocking agent should be carefully chosen for blocking these unreacted $–NH_2$ groups on the surface to prevent the directly adsorption of DNA strands onto the gold surface.

Other than that, by analyzing the peak separation and its dependence on the scan rate, this system can be used for studying the charge transfer process through biomolecules.

References

(1) Goodsterin, M. P. Interpretation of Oxidation-Reduction. *J. Chem. Educ.* **1970**, *47*, 452–457.

(2) Kolb, D. The Chemical Equation Part I: Simple Reactions. *J. Chem. Educ.* **1978**, *55*, 326–331.

(3) Zumdahl, S.; DeCoste, D. J. *Chemical Principles*; 7th ed.; Brooks/Cole, Cengage Learning: Belmont, CA, 2013.

(4) Marcus, R. a. On the Theory of Oxidation-Reduction Reactions Involving Electron Transfer. I. *J. Chem. Phys.* **1956**, *24*, 966.

(5) Harris, D. C. *Quantitative Chemical Analysis*; 8th ed.; W.H. Freeman and Co.: New York, NY, 2010.

(6) Kelly, J. J.; Xia, X. H.; Ashruf, C. M. A.; French, P. J. Galvanic Cell Formation: A Review of Approaches to Silicon Etching for Sensor Fabrication. *IEEE Sens. J.* **2001**, *1*, 127–142.

(7) Kim, H.; Boysen, D. A.; Newhouse, J. M.; Spatocco, B. L.; Chung, B.; Burke, P. J.; Bradwell, D. J.; Jiang, K.; Tomaszowska, A. A.; Wang, K.; *et al.* Liquid Metal Batteries: Past, Present, and Future. *Chem. Rev.* **2013**, *113*, 2075–2099.

(8) Mabbott, G. A. An Introduction to Cyclic Voltammetry. *J. Chem. Educ.* **1983**, *60*, 697–702.

(9) Kissinger, P. T.; Heineman, W. R. Cyclic Voltammetry. *J. Chem. Educ.* **1983**, *60*, 702–706.

(10) Bard, Allen J.; Faulkner, L. R. *Electrochemical Methods: Fundamentals and Applications*; 2nd ed.; John Wiley & Sons, Inc., 2001.

(11) Sassolas, A.; Leca-Bouvier, B. D.; Blum, L. J. DNA Biosensors and Microarrays. *Chem. Rev.* **2008**, *108*, 109–139.

(12) Joshi, T. A. Electrochemical Labeling and Detection of Dna : Recent Advances. *Int. J. Res. Pharm. Chem.* **2011**, *1*, 1015–1027.

(13) Zhang, B.; Liu, B.; Chen, G.; Tang, D. Redox and Catalysis “all-in-One” Infinite Coordination Polymer for Electrochemical Immunosensor of Tumor Markers. *Biosens. Bioelectron.* **2015**, *64*, 6–12.

(14) Steel, A. B.; Herne, T. M.; Tarlov, M. J. Electrochemical Quantitation of DNA Immobilized on Gold. *Anal. Chem.* **1998**, *70*, 4670–4677.

(15) Herne, T. M.; Tarlov, M. J. Characterization of DNA Probes Immobilized on Gold Surfaces. *J Am Chem Soc* **1997**, *119*, 8916–8920.

(16) Radi, A.-E.; Sánchez, J. L. A.; Baldrich, E.; O’Sullivan, C. K. Reusable Impedimetric Aptasensor Complex Formed between the Aptamer and Thrombin Using. *Anal. Chem.* **2005**, *77*, 6320–6323.

(17) Lai, R. Y.; Seferos, D. S.; Heeger, A. J.; Bazan, G. C.; Plaxco, K. W. Comparison of the Signaling and Stability of Electrochemical DNA Sensors Fabricated from 6- or 11-Carbon Self-Assembled Monolayers. *Langmuir* **2006**, *22*, 10796–10800.

(18) Pheeney, C. G.; Barton, J. K. DNA Electrochemistry with Tethered Methylene Blue. *Langmuir* **2012**, *28*, 7063–7070.

(19) Ihara, T.; Maruo, Y.; Takenaka, S.; Takagi, M. Ferrocene-Oligonucleotide Conjugates for Electrochemical Probing of DNA. *Nucleic Acids Res.* **1996**, *24*, 4273–4280.

(20) Tortolini, C.; Bollella, P.; Antonelli, M. L.; Antiochia, R.; Mazzei, F.; Favero, G. DNA-Based Biosensors for Hg2+ Determination by Polythymine–methylene Blue Modified Electrodes. *Biosens. Bioelectron.* **2015**, *67*, 524–531.

(21) Ren, K.; Wu, J.; Ju, H.; Yan, F. Target-Driven Triple-Binder Assembly of MNAzyme for Amplified Electrochemical Immunosensing of Protein Biomarker. *Anal. Chem.* **2015**, *87*, 1694–1700.

(22) Ma, F.; Ho, C.; Cheng, A. K. H.; Yu, H.-Z. Immobilization of Redox-Labeled Hairpin DNA Aptamers on Gold: Electrochemical Quantitation of Epithelial Tumor Marker Mucin 1. *Electrochim. Acta* **2013**, *110*, 139–145.

(23) Barton, J. K. Simple Coordination Complexes: Drugs and Probes for DNA Structure. *Comments Inorg. Chem.* **1985**, *3*, 321–348.

(24) Carter, M. T.; Bard, A. J. Voltammetric Studies of the Interaction of Tris(1,10-Phenanthroline) cobalt(III) with DNA. *J. Am. Chem. Soc.* **1987**, *109*, 7528–7530.

(25) Carter, M. T.; Rodriguez, M.; Bard, A. J. Voltammetric Studies of the Interaction of Metal Chelates with DNA. 2. Tris-Chelated Complex of Cobalt (III) AND Iron (II) with 1,10-Phenanthroline and 2,2’-Bipyridine. *J. Am. Chem. Soc.* **1989**, *111*, 8901–8911.

(26) Pang, D.-W.; Abruña, H. D. Micromethod for the Investigation of the Interactions between DNA and Redox-Active Molecules. *Anal. Chem.* **1998**, *70*, 3162–3169.

(27) Armor, John N, Scheidegger, Hans A, and Taube, H. A Bimolecular Mechanism for Substitution. *J. Am. Chem. Soc.* **1968**, *90*, 5928–5929.

(28) Castillo-Villalon, P.; Ramirez, J.; Peltre, M.-J.; Louis, C.; Massiani, P. An UV-Visible Study of the Stability of the Ruthenium Hexaammine Cation in BEA Zeolites?comparison with NaY. *Phys. Chem. Chem. Phys.* **2004**, *6*, 3739–3746.

(29) Yu, H.-Z.; Luo, C.-Y.; Sankar, C. G.; Sen, D. Voltammetric Procedure for Examining DNA-Modified Surfaces: Quantitation, Cationic Binding Activity, and Electron-Transfer Kinetics. *Anal. Chem.* **2003**, *75*, 3902–3907.

(30) Ge, B.; Huang, Y.-C.; Sen, D.; Yu, H.-Z. Electrochemical Investigation of DNA-Modified Surfaces: From Quantitation Methods to Experimental Conditions. *J. Electroanal. Chem.* **2007**, *602*, 156–162.

(31) Su, L.; Sen, D.; Yu, H.-Z. Voltammetric Study of the Ion-Exchange Binding of Non-Electroactive Metal Cations to DNA-Modified Surfaces. *Analyst* **2006**, *131*, 317–322.

(32) Cheng, A. K. H.; Ge, B.; Yu, H.-Z. Aptamer-Based Biosensors for Label-Free Voltammetric Detection of Lysozyme. *Anal. Chem.* **2007**, *79*, 5158–5164.

(33) Mayer, G. The Chemical Biology of Aptamers. *Angew. Chemie - Int. Ed.* **2009**, *48*, 2672–2689.

(34) Wild, D. *The Immunoassay Handbook*; 3rd ed.; Elsevier Science: London, 2005.

(35) Schwardt, O.; Kolb, H.; Ernst, B. Drug Discovery Today. *Curr. Top. Med. Chem.* **2003**, *3*, 1–9.

(36) Morris, B. A.; Clifford, M. N. *Immunoassays in Food Analysis*; Elsevier: London, 1985.

(37) Knopp, D. Immunoassay Development for Environmental Analysis. *Anal. Bioanal. Chem.* **2006**, *385*, 425–427.

(38) Heineman, W. R.; Halsall, H. B. Strategies for Electrochemical Immunoassay. *Anal. Chem.* **1985**, *57*, 1321A – 1331A.

(39) Lequin, R. M. Enzyme Immunoassay (EIA)/enzyme-Linked Immunosorbent Assay (ELISA). *Clin. Chem.* **2005**, *51*, 2415–2418.

(40) Engvall, E.; Perlmann, P. Enzyme-Linked Immunosorbent Assay (ELISA) Quantitative Assay of Immunoglobulin G. *Immunochemistry* **1971**, *8*, 871–874.

(41) Josephy, P. D.; Eling, T.; Mason, R. P. The Horseradish Peroxidase-Catalyzed Oxidation of 3,5,3',5'- Tetramethylbenzidine. *J. Biol. Chem.* **1982**, *257*, 3669–3675.

(42) Burns, R. *Immunochemical Protocols*; 3rd ed.; Humana Press, 2005.

(43) Zhu, S.; Zhang, Q.; Guo, L. H. Part-per-Trillion Level Detection of Estradiol by Competitive Fluorescence Immunoassay Using DNA/dye Conjugate as Antibody Multiple Labels. *Anal. Chim. Acta* **2008**, *624*, 141–146.

(44) Zhang, Q.; Guo, L.-H. Multiple Labeling of Antibodies with Dye / DNA Conjugate for Sensitivity. *Bioconjugate Chem.* **2007**, *18*, 1668–1672.

(45) Chikkaveeraiah, B. V.; Mani, V.; Patel, V.; Gutkind, J. S.; Rusling, J. F. Microfluidic Electrochemical Immunoarray for Ultrasensitive Detection of Two Cancer Biomarker Proteins in Serum. *Biosens. Bioelectron.* **2011**, *26*, 4477–4483.

(46) Hou, L.; Wu, X.; Chen, G.; Yang, H.; Lu, M.; Tang, D. HCR-Stimulated Formation of DNAzyme Concatamers on Gold Nanoparticle for Ultrasensitive Impedimetric Immunoassay. *Biosens. Bioelectron.* **2015**, *68*, 487–493.

(47) Filippov, N. S.; Lomzov, A. A.; Pyshnyi, D. V. Thermodynamic Description of Oligonucleotide Self-Association in DNA Concatamer Structures. *Biophysics (Oxf).* **2009**, *54*, 280–290.

(48) Chikkaveeraiah, B. V.; Bhirde, A. A.; Morgan, N. Y.; Eden, H. S.; Chen, X. Electrochemical Immunosensors for Detection of Cancer Protein Biomarkers. *ACS Nano* **2012**, *6*, 6546–6561.

(49) Zhang, S.; Zheng, F.; Wu, Z.; Shen, G.; Yu, R. Highly Sensitive Electrochemical Detection of Immunospecies Based on Combination of Fc Label and PPD Film/gold Nanoparticle Amplification. *Biosens. Bioelectron.* **2008**, *24*, 129–135.

(50) Tang, D.; Ren, J. In Situ Amplified Electrochemical Immunoassay for Carcinoembryonic Antigen Using Horseradish Peroxidase-Encapsulated Nanogold Hollow Microspheres as Labels. *Anal. Chem.* **2008**, *80*, 8064–8070.

(51) Tran, H. V.; Piro, B.; Reisberg, S.; Huy Nguyen, L.; Dung Nguyen, T.; Duc, H. T.; Pham, M. C. An Electrochemical ELISA-like Immunosensor for miRNAs Detection Based on Screen-Printed Gold Electrodes Modified with Reduced Graphene Oxide and Carbon Nanotubes. *Biosens. Bioelectron.* **2014**, *62*, 25–30.

(52) Zhang, J.; Chen, X.; Yang, M. Enzyme Modified Peptide Nanowire as Label for the Fabrication of Electrochemical Immunosensor. *Sensors Actuators, B Chem.* **2014**, *196*, 189–193.

(53) Wang, Q.; Song, Y.; Chai, Y.; Pan, G.; Li, T.; Yuan, Y.; Yuan, R. Electrochemical Immunosensor for Detecting the Spore Wall Protein of Nosema Bombycis Based on the Amplification of hemin/G-Quadruplex DNAzyme Concatamers Functionalized Pt at Pd Nanowires. *Biosens. Bioelectron.* **2014**, *60*, 118–123.

(54) Yang, L.; Zhao, H.; Fan, S.; Deng, S.; Lv, Q.; Lin, J.; Li, C.-P. Label-Free Electrochemical Immunosensor Based on Gold-Silicon Carbide Nanocomposites for Sensitive Detection of Human Chorionic Gonadotrophin. *Biosens. Bioelectron.* **2014**, *57*, 199–206.

(55) Liu, Y.; Liu, Y.; Feng, H.; Wu, Y.; Joshi, L.; Zeng, X.; Li, J. Layer-by-Layer Assembly of Chemical Reduced Graphene and Carbon Nanotubes for Sensitive Electrochemical Immunoassay. *Biosens. Bioelectron.* **2012**, *35*, 63–68.

(56) Liu, L.; Li, Y.; Tian, L.; Guo, T.; Cao, W.; Wei, Q. A Label-Free Voltammetric Immunoassay Based on 3D-Structured rGO–MWCNT–Pd for Detection of Human Immunoglobulin G. *Sensors Actuators B Chem.* **2015**, *211*, 170–176.

(57) Yang, S. Y.; Chang, K. H.; Lee, Y. F.; Ma, C. C. M.; Hu, C. C. Constructing a Hierarchical Graphene-Carbon Nanotube Architecture for Enhancing Exposure of Graphene and Electrochemical Activity of Pt Nanoclusters. *Electrochem. commun.* **2010**, *12*, 1206–1209.

(58) Sun, T.; Zhang, Z.; Xiao, J.; Chen, C.; Xiao, F.; Wang, S.; Liu, Y. Facile and Green Synthesis of Palladium Nanoparticles-Graphene-Carbon Nanotube Material with High Catalytic Activity. *Sci. Rep.* **2013**, *3*, 2527–2533.

(59) Chen, Z. P.; Peng, Z. F.; Luo, Y.; Qu, B.; Jiang, J. H.; Zhang, X. B.; Shen, G. L.; Yu, R. Q. Successively Amplified Electrochemical Immunoassay Based on Biocatalytic Deposition of Silver Nanoparticles and Silver Enhancement. *Biosens. Bioelectron.* **2007**, *23*, 485–491.

(60) Lapthorn, A. J.; Harris, D. C.; Littlejohn, A.; Lustbader, J. W.; Canfield, R. E.; Machin, K. J.; Morgan, F. J.; Isaacs, N. W. Crystal Structure of Human Chorionic Gonadotropin. *Nature* **1994**, *369*, 455–461.

(61) Montagnana, M.; Trenti, T.; Aloe, R.; Cervellin, G.; Lippi, G. Human Chorionic Gonadotropin in Pregnancy Diagnostics. *Clin. Chim. Acta* **2011**, *412*, 1515–1520.

(62) Cole, L. A. Immunoassay of Human Chorionic Gonadotropin, Its Free Subunits, and Metabolites. *Clin. Chem.* **1997**, *43*, 2233–2243.

(63) Chard, T. Pregnancy Tests: A Review. *Hum. Reprod.* **1992**, *7*, 701–710.

(64) Stenman, U. H.; Tiitinen, A.; Alfthan, H.; Valmu, L. The Classification, Functions and Clinical Use of Different Isoforms of HCG. *Hum. Reprod. Update* **2006**, *12*, 769–784.

(65) Gubala, V.; Harris, L. F.; Ricco, A. J.; Tan, M. X.; Williams, D. E. Point of Care Diagnostics: Status and Future. *Anal. Chem.* **2012**, *84*, 487–515.

(66) Li, X.; Weng, S.; Ge, B.; Yao, Z.; Yu, H.-Z. DVD Technology-Based Molecular Diagnosis Platform: Quantitative Pregnancy Test on a Disc. *Lab Chip* **2014**, *14*, 1686–1694.

(67) Cole, L. A. *Quantitative hCG Assays in Human Chorionic Gonadotropin (hCG)*; Elsevier Insights: Burlington, USA, 2010.

(68) Bidart, J. M.; Birken, S.; Berger, P.; Kichevsky, A. Immunochemical Mapping of hCG and hCG-Related Molecules. *Scand. J. Clin. Lab. Invest.* **1993**, *53*, 118–136.

(69) Pang, D.-W.; Abruna, H. D. Interactions of Benzyl Viologen with Surface-Bound Single- and Double-Stranded DNA. *Anal. Chem.* **2000**, *72*, 4700–4706.

(70) Cole, L. A.; Ladner, D. G. Background hCG in Non-Pregnant Individuals: Need for More Sensitive Point-of-Care and over-the-Counter Pregnancy Tests. *Clin. Biochem.* **2009**, *42*, 168–175.

(71) Tawa, K.; Kondo, F.; Sasakawa, C.; Nagae, K.; Nakamura, Y.; Nozaki, A.; Kaya, T. Sensitive Detection of a Tumor Marker, α-Fetoprotein, with a Sandwich Assay on a Plasmonic Chip. *Anal. Chem.* **2015**, *87*, 3871–3876.

(72) Rucker, V. C.; Havenstrite, K. L.; Herr, A. E. Antibody Microarrays for Native Toxin Detection. *Anal. Biochem.* **2005**, *339*, 262–270.

(73) Vareiro, M. M. L. M.; Liu, J.; Knoll, W.; Williams, D.; Jenkins, A. T. A. Surface Plasmon Fluorescence Measurements of\rHuman Chorionic Gonadotrophin: Role of Antibody\rOrientation in Obtaining Enhanced Sensitivity and\rLimit of Detection. *Anal. Chem.* **2005**, *77*, 2426–2431.

(74) Englebienne, P. Use of Colloidal Gold Surface Plasmon Resonance Peak Shift to Infer Affinity Constants from the Interactions between Protein Antigens and Antibodies Specific for Single or Multiple Epitopes. *Analyst* **1998**, *123*, 1599–1603.

(75) Tan, Y. H.; Liu, M.; Nolting, B.; Go, J. G.; Gervay-Hague, J.; Liu, G. Y. A Nanoengineering Approach for Investigation and Regulation of Protein Immobilization. *ACS Nano* **2008**, *2*, 2374–2384.